POLITECNICO DI TORINO

Master's Degree in Energy Engineering

Master's Degree Thesis

Aqueous organic redox-flow batteries: experimental and techno-economic analysis

Supervisors

Andrea LANZINI

Francesco Demetrio MINUTO

Alessandro PEROL

Candidate

Filippo ANGARANO

2022-2023

Acknowledgements

My total gratitude to my whole family, whose unconditional support sustained throughout every hardships, they're my unwavering foundation and the wind upon my sails.

My heartfelt gratitude to Alessandro Perol, Marco Zampolli and Massimiliano Bindi. They showed me how experience and curiosity keep enthusiasm alive.

Special thanks to Ecem Sezginer, harbinger of hope and perennial source of inspiration. Her support has been fundamental and irreplaceable.

A huge "thank you" to Vincenzo Di Stasio, for being the best roommate I could ever ask for.

My grateful thanks to Sophia Eugenia Hodgkinson, for her unbreakable spirit and the permanent trace she left on my vision of the world.

My deep thanks to Professor Andrea Lanzini and Francesco Demetrio Minuto, for their support to this work's completion.

Many thanks to Simone Paliani, Gianluca Bussolo and Luca Morena, amazing comrades for an unforgivable first working experience.

Table of Contents

List of Tables V

List of Figures VI

Acronyms XIII

1 Introduction 1
- 1.1 Background and objective 1
- 1.2 Renewable energy sources: overview 2
- 1.3 Energy storage: characteristics 5
- 1.4 Redox-flow batteries: state of the art 8
  - 1.4.1 RFBs' constitutive elements 8
  - 1.4.2 RFBs: operation and features 10
  - 1.4.3 Vanadium-based RFBs: description and applications 11
  - 1.4.4 Polarization considerations for VRFBs 13
  - 1.4.5 Electrodes considerations for VRFBs 14
  - 1.4.6 Membranes' aspects in VRFBs 15
  - 1.4.7 Flow channels design considerations in VRFBs 15
  - 1.4.8 Critical aspects concerning VRFBs 17
- 1.5 Aqueous organic RFBs: innovative features 17
  - 1.5.1 Electrochemical considerations about AORFBs 18
  - 1.5.2 AORFBs' innovative aspects and potential 19

2 Methodology 21
- 2.1 Experimental setup 21
  - 2.1.1 Laboratory Environment 21
  - 2.1.2 Battery system and software's technical specifications 24
- 2.2 Techno-economic model 33
  - 2.2.1 Cost estimation approach 33
  - 2.2.2 Costs invoices breakdown 34

3 Results and discussion 44
- 3.1 Experimental analysis 44
  - 3.1.1 Performed tests typologies 44
  - 3.1.2 Final experimental considerations 60
- 3.2 Techno-economic results 61
  - 3.2.1 AORFB results 61
  - 3.2.2 Comparison between AORFB and VRFB results 62

4 Conclusions 68

A Techno-economic features 70

B Python Code 72

Bibliography 76

List of Tables

1.1 Table of energy storage systems (ESS) technologies' characteristics [17]. The main ESS typologies are differentiated depending on the form of energy converted: electro-magnetic (in yellow), mechanical (orange), electrochemical (in green), and chemical (in blue). 7

3.1 Direct current (DC) average Efficiencies values for different reduced state of charge (SOC) ranges: The experimental values prove how the main influence on the AORFB's performance lies in the application's power level. 58

3.2 Techno-economic results for different power sizes and roundtrip efficiencies scenarios. While CAPEX and OPEX values are the same, the increase of RTE significantly reduces the LCOS values. 62

List of Figures

1.1 Renewable annual net capacity additions by technology, main and most optimistic (accelerated) cases, 2015-2027. The forecast yearly RENs' capacity additions are expected to increase continuously over the forecast period, reaching a maximum of 460 GW in 2027 in the main case. PV and wind provide the highest majority of global RENs capacity increase [4]. 3

1.2 Schematic of RFB's stack elements[29]. The ions move across the membrane, and redox reactions occur at the interface between electrodes and electrolyte, flowing within the flow fields. In the bipolar plates, the redox electrons are collected and sent to the external circuit, to be used for energy applications. 9

1.3 VRFB scheme [28]. The organic active species are dissolved in the catholyte and anolyte, which are pumped from their respective tanks tanks into the stack cells. During the redox reactions in the cells, the ions movement across the membrane, and the redox electrons are collected and sent to the external circuit. Since RFBs operate at direct current and low direct voltage, a DC/DC converter raises the voltage level and DC/AC converter is used towards external electric devices. 10

1.4 Dalian's 100 MW/400 MWh VRFB battery system, connected to China's natinal electric grid on October 2022 and operative ever since. Currently, this constitutes the world's largest redox-flow battery system on an industrial scale. 12

1.5 Polarization curve for electrochemical batteries, with displayed overvoltage losses: Activation, due to charge transfer phenomena at the electrodes; Ohmic, due to charge transport phenomena; Concentration, due to mass transport phenomena of molecules diffusion [29]. 14

1.6 Flow configurations:"flow-through" (left) and "flow-by" (right) [29]. The "flow-through" configuration is the traditional technological solution for flow channels. In the "flow-by" setting, the flow channels are directly machined into the bipolar plates. 16

1.7 Flow configurations: serpentine flow field (left) and inter-digitated (right) [29]. Serpentine flow field is used to minimize pressure losses and the thickness of the electrode; in the inter-digitated flow field, the electrolyte flows perpendicularly with respect to the channels. . 16

2.1 Plan view of the AORFB device in the Officine Edison laboratory . 21

2.2 Switchboard workplace, interface with the AORFB. Here, the electronic load is located, as well as the computer to interface with the battery device and the general supply selector. 23

2.3 Parameters of the electronic three-phase and generator load 23

2.4 AORFB's prototype device and interface workplace, shown during the battery installation phase. 24

2.5 Battery device's visual rendering, given by the battery provider. . . 25

2.6 Battery's stack components view, given by the battery provider. The electrolytes'inlet and outles are shown, as well as the disposition of the cells' membranes, bipolar plates and felts within the stack, with the current collectors on the sides. 25

2.7 Battery device's parameters, given by the technology provider. In here, the operational limits of voltage, temperature and state of charge are shown. 25

2.8 AORFB system's electric scheme, shared by the technology provider. 26

2.9 AORFB's electric blocks connections, where the three stacks are shown, electrically connected in parallel. The DC/DC converter is necessary to increase the battery's output low voltage. The power conversion system (PCS) not only regulates the AC/DC converter, while PMS is the interface controls PCS and BMS, and applies current and power limitations. 26

2.10 AORFB system's hydraulic scheme, shared by the technology provider. The many pressure sensors and valves are illustrated, indicating the main monitored pressure values in the cells, pipes, and tanks. . . . 27

2.11 AutoCAD's rendering of the AORFB hydraulic connections, depicting the counter-flow flowing of the electrolytes. The main pressure valves on the tanks, determining the controlling setting's value, are illustrated here. 28

2.12 LabVIEW's adopted settings. The most crucial parameters are represented by the upper and lower SOC limits. The battery's cycles do not start until SOC lies within the indicated limits. On the other hand, the logging period indicates the database acquisition time for the experimental measures. 30

2.13 LabVIEW's front panel example profile. The power values are inserted here, where negative positive and inputs apply a cycle of charge and discharge, respectively. Each cycle's duration is set via the respective time input. 31

2.14 LabVIEW's front panel display. The stacks' profile of current and voltage are shown on the left, as well as the real-time measured SOC level. The bottom-right side shows the power profiles of the battery devices, of the auxiliary consumption and of the overall system. The values of electrolytes' temperature and pressure within the cells are displayed as well, together with some sensors to detect eventual faults in the PCS or BMS. 32

2.15 VRFB costs percentages and invoices values. The percentages indicated in [37] are applied to the overall costs provided in [32], obtaining the specific values of the individual cost voices, especially the electrolyte's value. 35

2.16 AORFB costs percentages. The overall costs sum value has been hsared by the technology providers, while the same cost values for the same 8 sub-voices used for VRFB have been kept constant. Then, the individual percentages have been obtained, and used to calculate the organic electrolyte value. The new organic electrolyte is circa 70% lower than the average one for vanadium batteries, thus reducing this component's impact on the battery's overall expenses. 36

2.17 Trends of SB, BOS and System Integration invoices. The displayed graphs, obtained from MatLab's cftool, visually show the accuracy of the adopted formulae to represent these trends, to get the invoices' values for any power input values between 10 kW and 100 MW. . . 38

2.18 Goodness of fit coefficients of cftool's trends. All the values of R-square are very close to 1, proving the trend's high accuracy. The RMSE (Root Mean Square Error) low values indicate a low discrepancy between the reference values and the ones of the trends'. Finally, SSE (Sum of Square Errors) low values express a low sum of squared residuals, and the consequent trends' validity. 38

2.19 Conceptual map of the cost calculation steps. The cost related to power only are multiplied by P_n. Among the cost depending of energy capacity, System Integration and BOS values are the same as VRFB's four hours reference values from [32], since they don't vary with discharge duration tn. From SB, on the other hand, Tanks and electrolyte costs depend on the application duration and are multiplied for tn. Once all the costs are referred to monetary unit of measurement [\$], the actual CF_0 and CF_{12} are obtained, and Capex can be calculated. 43

3.1 Cell's direct voltage (V_{dc}) and Open-Circuit Voltage (OCV) with respect to the state of charge SOC, at low power rate C/6. The trends of V_{dc} and OCV show the system's electrochemical stability. 45

3.2 Cell's direct voltage (V_{dc}) and Open-Circuit Voltage (OCV) with respect to the state of charge SOC, at higher power rate C/1. As discussed hereafter, the imposed power derating sensitively affects the voltage trend. 46

3.3 Open-Circuit Voltage's trend (OCV) with respect to the state of charge (SOC), measured at low power rate C/6. The consistency of the OCV measures can be appreciated from the accurately overlapping charge and discharge curves. 46

3.4 Normalized trends of stack's direct current (I_{dc}), direct voltage (V_{dc}), and state of charge (SOC) at low power rate C/6. The currents trend is actually linear in both charge and discharge, with only few ampere of difference from the nominal value, even if here this difference may seem more impactful. 47

3.5 Normalized trends of stack's direct current (I_{dc}), direct voltage (V_{dc}), and state of charge (SOC) at high power rate C/1. Here the power derating imposed by the PCS is visually evident, showing the system's behavior when operating at specific values of SOC. 48

3.6 State of available power (SOAP) imposed by the PCS, with generators' sign representation (negative for charge, positive for dicharge). The SOAP provides a visual map of the derating imposed on the battery's operative behavior. 48

3.7 Derating verification curve. After being partially charged until 50% of SOC, the battery has been disconnected and immediately discharged. This test has showed that the derating is immediately activated as soon as the system is operative again, proving the actual operating power range and behavior. 49

3.8 State of available power (SOAP) curves for all the different evaluated C/rates over the full-DOD tests. The experimental campaign has verified the actual power operating area, which is slightly higher than the theoretical performance indicated by the technology's providers. 50
3.9 Battery's trend of the average recorded values of discharge ampere-hour [Ah] capacity, measured during the discharge phase. The cponsistent linear trend throughout the measured timeframes represents a further evidence of the electrochemical stability performance of the AORFB. 50
3.10 Average values' trend of direct current (DC) Energy, experimentally measured during the charging phase. The results show a very linear and stable trend for all the investigated nominal charging time durations. 51
3.11 Average values' trend of direct current (DC) Energy, experimentally recorded in the discharging phase. The results show a linear trend for time durations above 2 hours, with a decrease in value for lower discharge intervals. 51
3.12 Average experimentally measured values of direct current (DC) efficiency. The trend shows consistent values above 85% for discharge duration times higher than 2 hours, while below this threshold the efficiency is significantly reduced to circa 72%. This reduction is most probably due to lower electrodes' kinetics, occurring at higher power rates. 52
3.13 Average standard auxiliary consumption (AUX) trend, for both charge and discharge phases. The recorded results indicate how the auxiliary consumptions, with the highest contribution of pumping, is not linearly dependent on the battery's power rate. The high impact of AUX would be reduced with design optimization in s real-case device. 53
3.14 Auxiliary consumption (AUX), including heating devices activation for electrolytes' temperature below 21°C, and consequent significant auxiliary increase. As soon as the set temperature is reached, AUX value instantaneously returns to nominal values. 55
3.15 Reduced SOC interval tests at reduced state of charge (SOC). These tests evaluate the possible influence of SOC intervals on the device's performances. 56
3.16 Direct current (DC) average efficiencies values for different reduced state of charge (SOC) ranges. The experimental campaign showed how the efficiency results are quite consistent even at different SOC intervals. 57

3.17 Economic results for the studied device's size and discharge duration. Although it is a prototypal experimental system, the battery device studied in this model has been considered as a full AORFB system, evaluating all the techno-economic features considered in this model. 62
3.18 CAPEX and OPEX comparison between AORFB and VRFB, considering the power size variation. As expected, the expenditures of the organic technology records lower values with respect to vanadium-based devices, due to the drastic reduction of electrolyte cost. . . . 63
3.19 LCOS comparisons between AORFB and VRFB, at different roundtrip efficiency (RTE) values. Even accounting organic degradation, in order for AORFB to be competitive with VRFB, a minimum value of RTE=65% has to be provided. 64
3.20 LCOS comparison between VRFB and AORFB, with a sensitivity analysis on the eventual derating application. For nominal power sizes of 1, 10 and 10 MW, the applied derating reduces the produced energy up to 70% of nominal energy, with higher reductions for short-time applications. Accounting the derating for AORFBs, the LCOS value increases significantly, making organic technology less competitive than VRFB. However, derating procedures are decided by the technology providers to preserve the battery stability. Therefore, derating consists of a precautionary measure that, with increasing technological know-how, is destined to be removed in the near future. 65
3.21 LCOS results at different duration applications, for 1, 10 and 100 MW. The most competitive solutions include nominal discharge duration between 8 and 10 hours, where the energy factor is the dominant contribution over the expenditures factors. In these duration timeframes, the LCOS value is minimized. After 10 hours, the costs increase become predominant, causing a consequent aigmentation of the LCOS. Moreover, an increase of power size brings a further reduction of the costs, mostly due to economy of scale effects. 66

A.1 WACC parameters values 71

Acronyms

AC

Alternate current

AORFB

Aquoeus organic redox flow battery

AUX

Auxiliary consumption

BMS

Battery management system

BOS

Block of storage

CC

Control and communication

CF

Cash flow

COE

Cost of equity

DC

Direct current

DF

Debt fraction

DOD

Depth of discharge

ELY

Electrolyte

ESS

Energy storage system

EV

Electric vehicle

GHG

Greenhouse gases

LCOS

Levelized cost of storage

LDES

Long duration energy storage

OCV

Open-circuit voltage

PCS

Power conversion system

PNNL

Pacific Northwest National Laboratory

PV

Photovoltaic

RFB

Redox flow battery

REN

Renewable energy source

RMSE

Root mean square value

RTE

Roundtrip efficiency

SB

Storage block

SOC

State of charge

SMES

Superconductive magnetic energy storage systems

SSE

Sum of square errors

UN

United Nations

VRFB

Vanadium-based redox flow battery

WACC

Weighted average cost of capital

Abstract

In the recent years' pursue of affordable and high-performing energy storage devices, redox-flow batteries have shown great potential for long-duration operations.

With cheaper and more environmentally-sustainable materials with respect to more mature vanadium-based devices, aqueous organic redox flow batteries (AORFBs) currently constitute the research focus to bring out the full potential of redox-flow technology.

Hovewer, due to being an innovative technology, AORFBs behavior has yet to be investigated deeply, both from an operational and from a techno-economic point of view.

In this work, an AOEFB prototype battery system device has been experimentally tested at Officine Edison Laboratory in Turin.

Numerous experimental tests have been carried out, to effectively assess the performances of an AORFB battery system in many operational conditions, for both deep depth of discharge and reduced state of charge ranges. Energy and efficiency results have being reported, as well as considerations of auxiliary consumptions' impacts on AORFBs' roundtrip efficiency.

Finally, a techno-economic analysis has been carried out, to evaluate the actual feasibility of AORFB devices. A comparison with vanadium-based technology has been highlighted, bringing peculiar considerations for possible near-future implementations.

The experimental campaign has shown AORFBs' high performance in long duration applications, with electrochemical efficiency values up to 86% in different state of charge conditions. Moreover, this work shows AORFBs' competitiveness with vanadium-based devices.

Chapter 1

Introduction

1.1 Background and objective

The following work has been focused on the study of an aqueous organic redox-flow battery device. This innovative technology is currently research focus all around the world, due to its sizing flexibility and potential characteristics of long cycle life and operative stability. An experimental campaign has been undertaken, to investigate the behavior of an organic redox-flow battery device system, to evaluate this technology's operational performances and effective capabilities. Main purpose of the experiments consisted in analyzing the operational stability of this innovative battery technology at different conditions of duration, power rates and state of charge conditions.

Moreover, a techno-economic analysis has been performed, to prove the feasibility of such devices and the most crucial aspects for their realization, and comparing the results of more innovative aqueous organic batteries with the most mature vanadium-based technology.

The motivation propelling this work resides in the ambition to prove how aqueous redox batteries provide remarkable characteristics for long-duration energy storage applications. Their operational stability, long cycle life and their sizing flexibility are key aspects to enhance the affirmation of renewable energy sources on a large-scale industrial level.

1.2 Renewable energy sources: overview

Energy production has always been a crucial topic: it is intrinsically rooted in technological progress, and it concerns every aspect of human needs and activities. In the last decade, with the aim of industry electrification and with the global affirmation of electric vehicles (EVs), the entirety of electricity-related processes, products and innovations, has been progressively and steadily increased. A higher energy and power consumption has been recorded, with an expected global energy demand increase of 5900 TWh by 2030 [1]. And with the parallel growth of human population, it is most probable to increase even more.
Accounting all the above, many urgent challenges arise:

1. Research for alternative energy sources and systems, to face upcoming depletion and consumption of raw materials and resources.
2. Reduction of greenhouse gas (GHG) emissions, for both current and future technological sectors, plants and industries, in order to avoid further temperature increase worsening the climate crisis' effects.
3. Ensure affordable and reliable access to energy services around the world.

To face all these challenges [2], The United Nations' (UNs') Sustainable Development Goal number 7 explicitly addresses the need to increase the share of renewable energy sources (RENs), which currently provide the most promising solution [3]. With the prices' increase of fossil fuels due to the global energy crisis, RENs have become more and more competitive, and their imminent affirmation worldwide is forecast to take place soon.
According to IEA [4], in the timeframe between 2022 and 2027, RENs are forecast to grow by 2.4 TW of installation, aiming to cover more than 90% of the expansion of electricity capacity and becoming the main electricity source by 2025. The penetration of RENs in the energy production mix is expected to reach almost 40% by 2027. The foreseen protagonists of this acceleration are China, India, the United States (US), and Europe, implementing policies and market regulations specifically addressing RENs' development, growth and management.
Due to public incentives and policies, as well as technological improvement, solar photovoltaic (PV) generation has become more and more economically affordable and reliable in providing services [5].
Currently, where geographically available, PV has become cheap enough to be competitive with traditional energy sources, especially with fossil fuels [6]. PV and wind, with their yearly steady increase, are expected to cover 80% of RENs generation worldwide by 2027, with a forecast capacity of 460 GW [7].
PV alone will cover 60% of global RENs production, with the major contribution in commercial and residential applications. Even if module prices have not lowered

since 2020, the current decrease in utility-scale installations in the majority of countries allows PV to constitute the least costly option for new electricity production solutions. Therefore, PV increasing power capacity is destined to surpass pumped hydroelectric, natural gas and coal by 2027 [4].

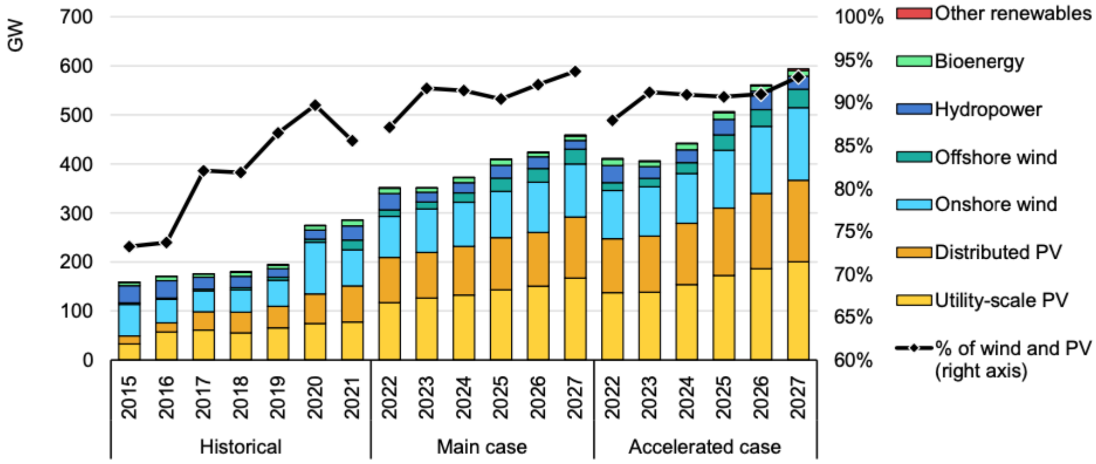

Figure 1.1: Renewable annual net capacity additions by technology, main and most optimistic (accelerated) cases, 2015-2027. The forecast yearly RENs' capacity additions are expected to increase continuously over the forecast period, reaching a maximum of 460 GW in 2027 in the main case. PV and wind provide the highest majority of global RENs capacity increase [4].

Wind production is expected to double by 2027, with an expected onshore capacity rising to 570 GW, even accounting the present time requirements for bureaucratic and permitting procedures, as well as infrastructural strengthening [8]. Onshore wind expansion requires stable regulatory frameworks, which ensure: long-term profitability, policies that facilitate permitting, and systemic grid and infrastructure enlargement and support. Offshore wind expansion is expected to increase to 30 GW by 2027, with the support of dedicated policies in Europe, China and US [9]. Obviously, the forecast increase in installed capacity can further increase, by realizing technical and infrastructural improvements, and implementing adequate policy regulations, to ensure the security and efficiency of power systems, both on a smaller and larger scale.

The main obstacles lie in permitting and grid implementations for most developed economies, in policy and regulations for emerging economies, and in a lack of infrastructures in developing economies. Currently, existing policies and market reforms have seen a first implementation in China, India, the US and Europe, and more reforms and subsidies plans are bound to happen in the next five years.

RENs' forecast growth in the upcoming years is currently supported by market trends and regulatory subsidies. However, the most needed support comes from technological stability. The natural intrinsic fluctuations of RENs results in an

inconstant energy generation, preventing them from guaranteeing continuity of generation, grid integration and an overall reliable service. This represents the main obstacle for their global further affirmation on a large-scale level, enabling to extract their full potential.
The best support to increase RENs' supply reliability, providing flexibility and effective demand satisfaction, lies in energy storage systems (ESSs).

1.3 Energy storage: characteristics

In recent years, many technical solutions have been investigated and tested to properly collect Renewable Energies sources' (RENs') generation surplus, in order to re-use it when the generation is lower or totally absent [10].
Moreover, Energy Storage Systems (ESSs) provide a strategic tool to increase RENs penetration in national grids, enabling to perform grid's capacity regulation and ancillary services like frequency regulation [11].
Depending on the chosen technology, ESSs provide different characteristics and performances [12]. Most of the main ESSs' properties to be considered are listed here:

1. Storage capacity: the capability to store energy for determined periods of time, with minimized materials' operational and calendar degradation (or "aging").
2. Power rating: indicating how much power the device can provide, and how fast the energy can be continuously and completely discharged.
3. Energy density and power density: expressing how much energy and power are stored with respect to ESSs' volume.
4. Roundtrip efficiency (RTE): parameter quantifying the amount of energy provided in the discharging phase with respect to the energy absorbed during charge. It indicates the quality of power and energy conversion, including all energy consumption and devices necessary for the whole ESS' system operation.
5. Operational and cycle lifetime: the actual device's life, expressed as years and/or number of cycles.
6. Response time: showing how quickly the power is provided, for a determined service and/or performance.
7. Levelized cost of storage (LCOS): expressing the cost that the ESS's unit of energy has to be sold at, in order to recover the investment; LCOS allows to compare the performances of different ESS technologies.
8. Scalability: indicating the ensemble of constitutive and technological features enabling a relatively easy devices' scaling-up and size increase, for large-scale applications.

The numerous ESS types and categories are differentiated by the form of intermediate energy deployed to store electricity [13].
Among the numerous types, the current main ESS categories [14] are indicated here:

1. Electrochemical, performing reversible redox reactions modifying the electronic asset of the ions to store electricity.
2. Mechanical, including systems storing electricity in the form of mechanical energy; main examples are such as pumped hydroelectric, compressed air or liquid air energy systems (CAES and LAES, respectively), and flywheels.
3. Magnetic, using devices like superconductive magnetic energy storage systems (SMES) that store electricity within magnetic fields produced by a superconductive coil.
4. Thermal, converting electricity into thermal energy, storing it as sensible or latent heat.
5. Chemical, where simple molecules are produced through electrolysis.

Among these categories, electrochemical ESSs, commonly named "batteries", are particularly remarkable for their modularity and performance [15].
Each battery consists of many fundamental constitutive cells, which are formed by two electrodes and a membrane. The membrane contains the electrolyte, which enhances the passage of a specifically charged ions' type from one electrode to the other, thus performing the redox reactions. The electrons involved in the reactions are carried from the electrode towards the external circuit, enabling the exchange of electric energy with external devices and/or systems.
Numerous cells are connected in series and/or in parallel, forming stacks, to obtain the desired values of current and voltage, depending on the needed operational characteristics. Since electrochemical devices operate in direct current (DC) conditions, the complete system also includes a conversion electric system from direct current (DC) to alternate current (AC).
Battery systems contain devices which are necessary to guarantee the operability and safety of the battery device throughout the system's whole life cycle. These devices are therefore named "auxiliary components", and present different elements depending on the battery's technology and constitutive characteristics.
Of course, the internal features of a battery determine the final electrochemical performance. Energy density and power density represent some of the most relevant internal parameters [16], and they can be calculated with the formulae 1.1 and1.2.

$$p_{\text{density}}[W/L] = \frac{I \cdot V}{volume} \tag{1.1}$$

$$e_{\text{density}}[Wh/L] = \int_0^t \frac{I \cdot V}{volume}\, dt \tag{1.2}$$

Where I represents the discharge current, V is the cell's output voltage, A symbolizes the electrode's active area and "*volume*" namely indicates the storage devices' volume. Electricity ESS provide numerous and different characteristics, not only among different technologies (chemical, electrical, mechanical, and thermal), but also between devices within the same category.

Here the comprehensive table 1.1 summarizes the main ESS technologies' characteristics [17]. Some technologies, first of all Lithium batteries, have recently seen significant development. Due to their high energy density and consequent light weight, Lithium batteries have been a key factor in the diffusion of EVs [18]. Moreover, since they are a relatively mature technology and usually provide an efficiency higher than 85%, Lithium batteries have seen numerous applications as residential energy storage, mostly associated with PV [19].

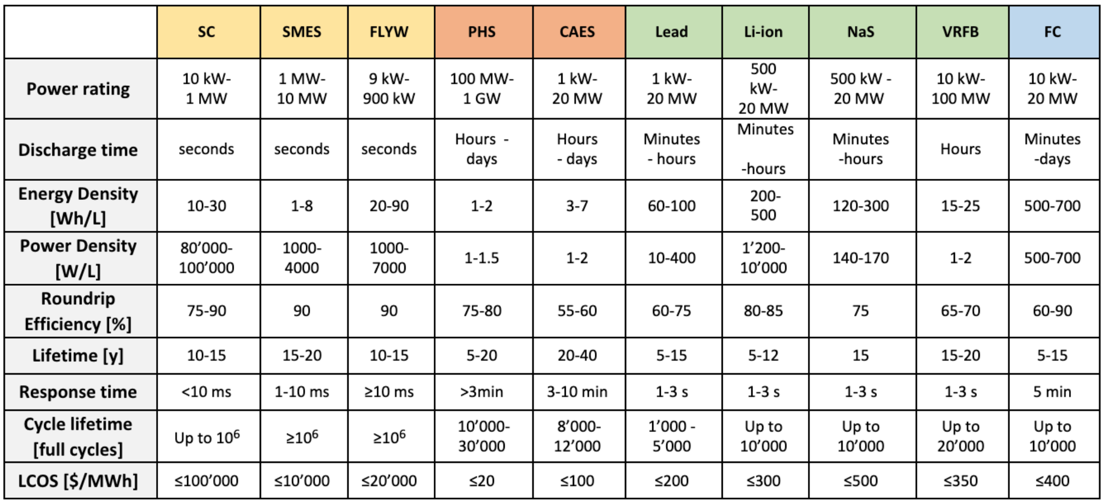

	SC	SMES	FLYW	PHS	CAES	Lead	Li-ion	NaS	VRFB	FC
Power rating	10 kW- 1 MW	1 MW- 10 MW	9 kW- 900 kW	100 MW- 1 GW	1 kW- 20 MW	1 kW- 20 MW	500 kW- 20 MW	500 kW - 20 MW	10 kW- 100 MW	10 kW- 20 MW
Discharge time	seconds	seconds	seconds	Hours - days	Hours - days	Minutes - hours	Minutes -hours	Minutes -hours	Hours	Minutes -days
Energy Density [Wh/L]	10-30	1-8	20-90	1-2	3-7	60-100	200- 500	120-300	15-25	500-700
Power Density [W/L]	80'000- 100'000	1000- 4000	1000- 7000	1-1.5	1-2	10-400	1'200- 10'000	140-170	1-2	500-700
Roundrip Efficiency [%]	75-90	90	90	75-80	55-60	60-75	80-85	75	65-70	60-90
Lifetime [y]	10-15	15-20	10-15	5-20	20-40	5-15	5-12	15	15-20	5-15
Response time	<10 ms	1-10 ms	≥10 ms	>3min	3-10 min	1-3 s	1-3 s	1-3 s	1-3 s	5 min
Cycle lifetime [full cycles]	Up to 10^6	≥10^6	≥10^6	10'000- 30'000	8'000- 12'000	1'000 - 5'000	Up to 10'000	Up to 10'000	Up to 20'000	Up to 10'000
LCOS [$/MWh]	≤100'000	≤10'000	≤20'000	≤20	≤100	≤200	≤300	≤500	≤350	≤400

Table 1.1: Table of energy storage systems (ESS) technologies' characteristics [17]. The main ESS typologies are differentiated depending on the form of energy converted: electro-magnetic (in yellow), mechanical (orange), electrochemical (in green), and chemical (in blue).

The current main obstacles for general ESS diffusion are:

1. High investment and/or maintenance costs.
2. Devices' aging and material degradation, if operating at non-nominal conditions.
3. Capacity oversizing, to try and cover higher demand, but causing inefficient operation.

Not even Lithium batteries currently provide the characteristics to fit all energy applications. Besides satisfying the base load, to ensure the coverage of instantaneous or temporary local peak demands, ESS devices need to be oversized [20]. This leads to short but repeated partial-load operating conditions, causing an inefficient

performance and inducing additional stress on the ESS system's materials, reducing the device's cycle life [21].
Moreover, Lithium battery's yearly degradation in operational conditions is usually around 2% [22], with a consequent cycle life between eight to ten years, which is usually inadequate for RENs timeframes like PV, with a plant life of more than 20 years.
In fact, in recent years the emerging topic involves Long Duration Energy Storage (LDES) systems. The definition of LDES encompasses conventional and novel technologies, with suitable characteristics to effectively store energy for time periods higher 6 hours [23]. Also, LDES should include the possibility to be easily scaled-up economically, to sustain electricity provision for days or even weeks [24].
Considering the challenges brought by the forecast of high RENs' penetration in the main current market scenarios [1], traditional battery systems will not suffice. Although they can be adapted and be suitable for both high energy and high power applications, even Lithium ion batteries present a cycle life incompatible with LDES necessities. At the same time, new market opportunities are currently arising for new technologies and innovative devices able to provide stable and reliable energy services and applications [25].
All the considerations accounted so far constitute the main reasons that have pushed researchers to investigate and test other ESS technologies for long-duration storage applications, leading to the investigation, in the last decade, of the core topic of this work: redox-flow batteries.

1.4 Redox-flow batteries: state of the art

Among the most promising electrochemical technologies, redox-flow batteries (RFBs) presents some unique features, suitable for long-duration applications. This technology, fruit of the research of Professor Maria Skyllas-Kazacos [26], was introduced to the scientific community in 1986. But it is only in the last decade that the potential of VRFBs has become of major interest, mostly because of RENs coupling [27].

1.4.1 RFBs' constitutive elements

RFBs' fundamental device consists of battery stacks, pumps, and two tanks. Each stack's cell consists of: [28]:

1. Two electrodes, usually made of modified carbon felts, where chemical redox reactions take place at the interface with electrolytes (ELYs).

2. Ion-conductive membrane separator, to allow the charges' movement but keeping the electrode's negative and positive sides separated.
3. Two graphite-based bipolar plates, where the electrons involved in the reactions are gathered to flow towards the external circuit in discharge charge operations.
4. Current collectors, to take the electrons exchanged during the redox reaction through the external circuit.
5. Gaskets, to mechanically seal the other components, and prevent electrolytes' leakage.

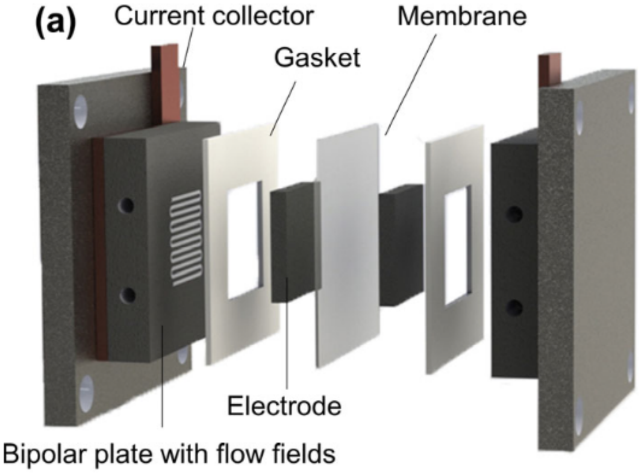

Figure 1.2: Schematic of RFB's stack elements[29]. The ions move across the membrane, and redox reactions occur at the interface between electrodes and electrolyte, flowing within the flow fields. In the bipolar plates, the redox electrons are collected and sent to the external circuit, to be used for energy applications.

1.4.2 RFBs: operation and features

The operation of RFBs is based on the exchange of electrical charges between molecules with different oxidation states. These molecules are dissolved within two liquid electrolyte solutions and pumped in the stack cells. One electrolyte flows through the anode side (thus, named "anolyte"), the other goes through the cathode (therefore named "catholyte"). While flowing within the cells, the two ELYs are separated by the ionic-exchanging membrane separator, which allows the ions' movement across the membrane during the redox reactions while avoiding the physical contact between fluids. At the electrodes, chemical energy is converted into electrical energy during the discharge phase, and viceversa in the charging process. After the exchange of electrons and ions in redox reactions, the two liquid ELYs are stored in tanks, physically detached from the stack.

The distinction between stack and tanks allows an independent sizing of power and energy, respectively. The battery's available power will be directly proportional to: the electrodes' area, the number of cells in the stack, and the number of stacks in the RFB system. Meanwhile, the amount of storable energy will be linearly dependent on the concentration of ELYs, and on the volume of ELYs stored in the tanks.

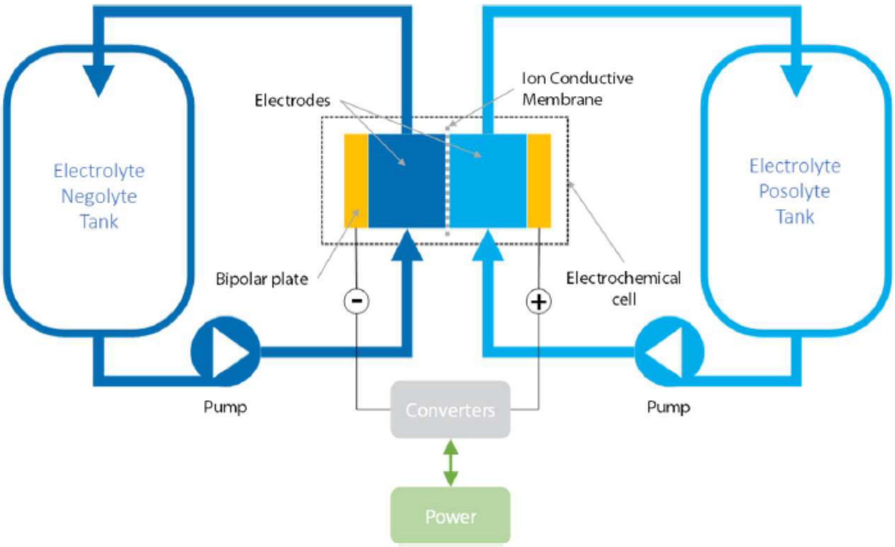

Figure 1.3: VRFB scheme [28]. The organic active species are dissolved in the catholyte and anolyte, which are pumped from their respective tanks tanks into the stack cells. During the redox reactions in the cells, the ions movement across the membrane, and the redox electrons are collected and sent to the external circuit. Since RFBs operate at direct current and low direct voltage, a DC/DC converter raises the voltage level and DC/AC converter is used towards external electric devices.

Depending on the desired application, energy and power sizes can be tailored with high flexibility, and this peculiarity constitutes one of the most interesting features of RFBs technologies. The physical separation between stack and tanks prevents secondary reactions when the battery is not operative (open-circuit conditions), thus minimizing the materials' aging and degradation within the stack, and the liquid solutions allow a long duration storage. Of course, RFBs produce direct current and low direct voltage, thus requiring a DC/DC converter to increase the voltage to the level of the device that the battery will be connected to, like an electric load or the grid.

RFBs' diffusion has yet to be affirmed, due to their current prices and because they're bulkier than traditional batteries. Obviously, due to their bulky system and necessary equipment, RFBs are more suitable for stationary applications. On the other hand, RFBs' molecules have a way lower energy density and power density compared to more mature ESS like Lithium-ion batteries. Nonetheless, not only RFBs provide great flexibility for both energy and power sizing, but their configuration to store chemical energy provides a very high durability and longer cycle lives, allowing a theoretical battery life of 20 years, much higher than more mature electrochemical ESSs' current best performances.

1.4.3 Vanadium-based RFBs: description and applications

The currently most mature RFB technology consists of Vanadium-based redox-flow batteries (VRFBs). Vanadium's atoms offer many possible oxidation states, with valid redox properties, and provides a very high chemical stability in acidic aqueous solutions. The possibilities introduced with VRFBs have been investigated since the late 1980s, and the potential of this technology has been focus of research for decades, before the energy storage topic got the visibility due to the global Energy Transition.

These reasons have allowed vanadium-based batteries to be the most mature redox-flow technology so far, both in research and industrial applications. In VRFBs, both electrode sides present reactions involving Vanadium ions, taking advantage of all Vanadium's different oxidation states. The following equations represent the reactions occurring at the negative and at the positive electrode side, respectively:

$$V^{3+} + e^- \rightleftharpoons V^{2+} \tag{1.3}$$

$$VO^{2+} + H_2O \rightleftharpoons VO_2^+ + 2H^+ + e^- \tag{1.4}$$

Even if the energy density of VRFBs, with average values of 25 Wh/L, is still way lower than more common Lithium batteries (between 200-500 Wh/L), Vanadium-based redox batteries have seen an increasing development in recent years, particularly as a possible alternative to Lithium batteries and pumped-hydro storage plants for long-duration energy storage solutions [30]. RFBs' potential is currently being explored, and this technology has recently seen a major increase in installed size devices for numerous energy applications. The largest RFB projects are the following, most of which are currently ongoing [31]:

1. Automobile Industrial Park, China: 100 MW/500 MWh, coupled with wind and PV.

2. Dalian City, China: 100 MW/400 MWh, for grid stability.

3. G&W Electric, USA: 2 MW/8 MWh: increasing grid reliability during peak demands.

4. Energy Superhub Project, UK: 2 MW/5 MWh: hybrid energy storage system, coupled with PV and Lithium-ion battery, for super-fast charge of EVs.

Figure 1.4: Dalian's 100 MW/400 MWh VRFB battery system, connected to China's natinal electric grid on October 2022 and operative ever since. Currently, this constitutes the world's largest redox-flow battery system on an industrial scale.

The following pages illustrate many key features determining redox-flow technologies' electrochemical performance, and addressing the current more mature hardware aspects to maximize these devices' performances.

1.4.4 Polarization considerations for VRFBs

To express the parameters affecting electrochemical battery's power density, and consequently their overall performance, the polarization curve and main voltage losses' components are here shortly presented. The Nernst equation is deployed to quantify the Open-Circuit Voltage E_{OCV}, i.e. the theoretical highest voltage value produced by the cell, as a function of the chosen active species.

$$E_{\text{OCV}}[V] = E^0 + \frac{R \cdot T}{z \cdot F} \cdot ln \frac{\prod_{r=1}^{R}[{C_r}^{\nu_r}]}{\prod_{k=1}^{K}[C_k^{\nu_k}]} \tag{1.5}$$

Where C_k and C_r represent the individual concentrations of the product and reactants respectively, each to the power of the single element's stoichiometric coefficient . E^0 is the electrode's standard potential. R indicates the universal gas constant, T is the temperature in [K]; z indicates the number of electrons exchanged in the overall chemical reaction, and F is the Faraday constant.

$$E_{\text{stack}} = N_{\text{cell}} \cdot E_{\text{OCV}} - E_{\text{loss}} \tag{1.6}$$

Where N_{cell} is namely the number of cells in a battery stack, and E_{loss} indicates the voltage losses occurring in the stack. The polarization curve is presented in figure 1.5.

For the vast majority of all electrochemical batteries, the main general polarization losses are:

1. Activation, from reaction kinetics of charge transfer towards the interface between electrodes and electrolytes.
2. Ohmic, due to charge transport limitations, mainly induced by cells' area of internal resistance, depending on the cell's material resistivity.
3. Concentration (or "Diffusion"), from mass transport effects, due to molecular diffusion of electrolytes' redox species at the electrodes.

Some considerations about hardware implementations are presented here, introducing research aspects explored in recent years to improve both ohmic and concentration polarizations behaviors.

Internal resistance of electrodes, plates, electrolytes, membranes and contact resistance between the components are the predominant factors of the ohmic polarization overvoltage contribution. But more details about the components give a better explanation of hardware components' influence and contribution to the global electrochemical performance.

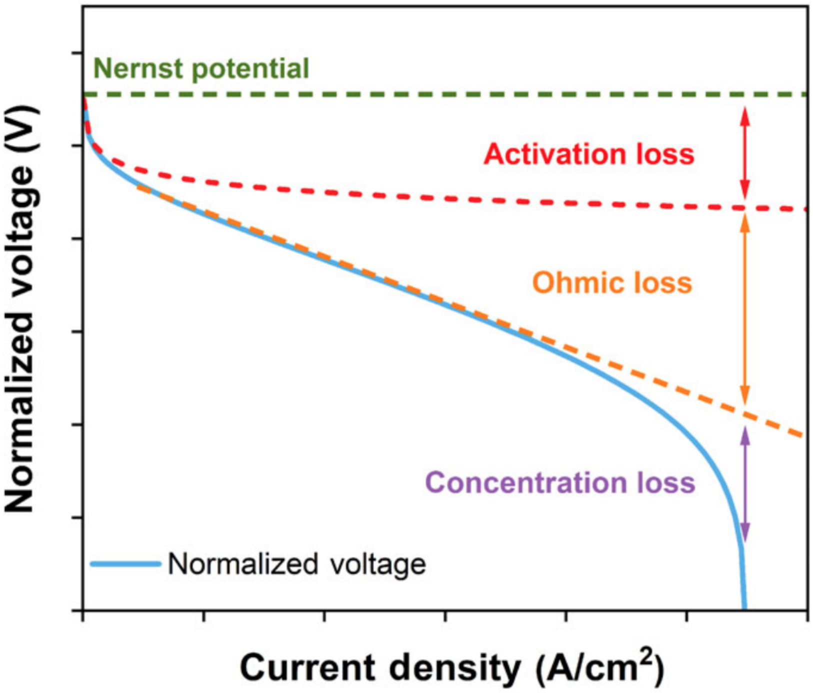

Figure 1.5: Polarization curve for electrochemical batteries, with displayed overvoltage losses: Activation, due to charge transfer phenomena at the electrodes; Ohmic, due to charge transport phenomena; Concentration, due to mass transport phenomena of molecules diffusion [29].

1.4.5 Electrodes considerations for VRFBs

The electrodes, as mentioned before, provide active reactions sites for the redox species dissolved in the ELYs. Referring to the polarization curve 1.5, electrodes' performance involve activation, ohmic and concentration overvoltages.

Optimal electrodes present high electrochemical activity, high ionic conductivity, low mass-transport resistance, and high structural stability. Carbon or graphite felts are the most commonly used electrodes' materials, since they minimize concentration and activation polarizations, due to their high porosity and high specific areas for the redox species involved in charge and discharge phases. Unfortunately, carbon felts usually present low electrochemical activity.

Many treatments can be applied to the eletrodes to boost their performances. Heat and chemical treatments (for example, nitrogen-containing groups treatments) are deployed to increase the energy efficiency and kinetics [29]. The energy efficiency boost effect is attributed to the oxygen functional groups' formation on the electrodes' area, where in this way the electrochemical reactions are enhanced.

The kinetics effect is attributed to the increase of redox species' affinity. Electrodes'

ohmic internal resistance mostly depends on porosity, tortuosity, thickness and internal resistive area. Metal electrodes have been investigated in many recent works (like Titanium-based and Nickel-based) [29], presenting high electronic conductivity and high electrochemical stability. However, their issues concerning corrosion, low surface area and significantly higher costs have prevented these components' large affirmation.
After electrodes, here there are some considerations on the component constituting the highest cost factor in RFBs' stacks: the membrane [32].

1.4.6 Membranes' aspects in VRFBs

An ion-exchange membrane acts as physical separators between catholyte and anolyte, to prevent cross-mixing of redox species, while allowing the passage of ionic charges through the membrane. The membrane's internal resistance accounts the biggest factor for the ohmic overvoltage.
The highest hardware cost today derives from membrane's preparation processes [32]: with impeccable quality preparation, the membrane must obtain a level of purity and constitutive properties able to guarantee high ionic conductivity and selectivity, ionic exchange capability, and of course stability.
Thinner membranes enhance lower ionic resistance, bringing higher power density and energy density, but in this way the ionic selectivity is reduced as well, causing crossover issues of redox species and consequent lower efficiency. A trade-off between high conductivity and high selectivity is therefore needed. Pre-treatments can enhance the membrane performances, and many processes are currently being focus of research and development studies.

1.4.7 Flow channels design considerations in VRFBs

The last hardware considerations involve the flow channels design. RFBs' most common architecture consists of porous electrodes pressed on a graphite plate. A uniform electrolytes' flow field's distribution inside the electrodes is essential to guarantee an effective forced convection mass transport and minimize the entity of the concentration overvoltage losses, otherwise a reduction of power density occurs.
The two main flow configurations are the "flow-through" and "flow-by". The "flow-through" is the traditional technological solution for flow channels design, while in the "flow-by" configuration the electrolyte is delivered to the electrode via flow channels machined within the bipolar plates. In recent works [29], the "flow-by" solution presented higher current density and peak power density with respect to traditional solutions, and more research activity is currently ongoing to explore all the characterizing aspects of this new configuration.

To reduce pressure drops within the flow channels in flow-through, an adequate electrode's thickness has to be designed, to reduce the ohmic losses caused by pressure losses. On the other hand, in a flow by mode the pressure drop is reduced if channels are adjacent to the electrodes.

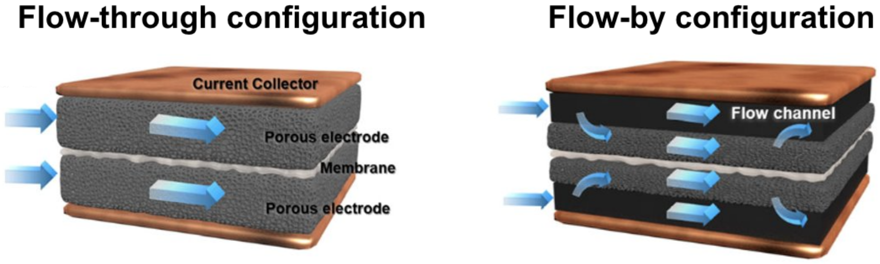

Figure 1.6: Flow configurations:"flow-through" (left) and "flow-by" (right) [29]. The "flow-through" configuration is the traditional technological solution for flow channels. In the "flow-by" setting, the flow channels are directly machined into the bipolar plates.

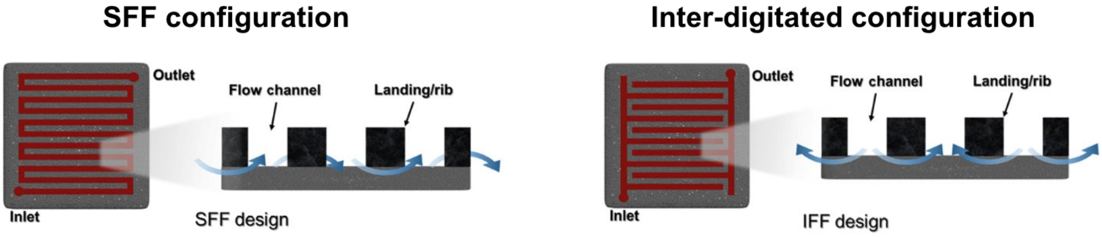

Figure 1.7: Flow configurations: serpentine flow field (left) and inter-digitated (right) [29]. Serpentine flow field is used to minimize pressure losses and the thickness of the electrode; in the inter-digitated flow field, the electrolyte flows perpendicularly with respect to the channels.

Another innovative setups have been recently explored in reseach work, to get best uniformity in the elecrolytes flow. The inter-digitated flow field configuration imposes an electrolyte's flow perpendicularly with respect to the channels. On the other hand, another channel configuration, serpentine flow field (SFF), is used to further reduce pressure losses while minimizing the electrodes' thickness. All these setups are currently research focus to find the best flow configuration.

As indicated in [29],higher electrolytes' flow rate seem to provide a more uniform flow distribution and decrease the concentration losses, thus increasing the performance. However, with higher auxiliary pumping consumption, the best trade-off between pumping consumption reduction and best flow distribution must be investigated to operate the best designing assumptions and realization processes, depending on the required operation conditions, considering electrolytes active species properties, flow design and application conditions altogether.

In conclusion, an optimized electrolytes' flow guarantees:

1. Reduction of the electrolytes' kinetics of diffusion, due to possible concentration gradients, and migration, due to electric gradient.
2. Uniform flow distribution, with consequent reduction of ohmic losses and better active material utilization.

1.4.8 Critical aspects concerning VRFBs

All the above-mentioned electrochemical characteristics and hardware implementations describe the main aspects to be faced during the designing phase of redox-flow technology.
Together with all the considerations described so far, there are some further aspects to be dealt with, specific of Vanadium-based devices. The main issues concerning VRFBs are the following [28]:

1. Vanadium's price volatility, hindering stable long-term investments.
2. Low thermal stability, with possible Vanadium precipitation into V_2O_5 at temperatures around 40°C [33], thus irreversibly reducing the electrolyte's operational activity.
3. Operation in highly acid conditions.
4. High Vanadium toxicity in solid form, therefore hazardous during electrolytes' preparation [34], requiring careful safety precautions and equipment.
5. Environmentally more hazardous to dispose at the devices' end-of life.

To face most of the above issues: aqueous organic redox-flow batteries have been investigated in the recent years, to implement a more sustainable redox-flow technology while providing promising performances.

1.5 Aqueous organic RFBs: innovative features

In this section, the main features of organic redox batteries are addressed, highlighting this technology's innovative characteristics. Aqueous organic redox-flow batteries share the same comprehensive functioning mechanisms of VRFBs, but deploying liquid solutions of organic molecules.
While "VRFB" is a univocal definition for a specific technology, the term "AORFB" indicates a family of technologies, since the variety of organic molecules that can be exploited for aqueous solution is potentially unlimited, as well as the redox couples that can be combined by modifying the structure of the chosen molecules.

Like VRFBs, aqueous organic batteries are influenced by chemical compositions, operational conditions and cell components' size and materials, although VRFBs currently present higher power density and energy density with respect to organic RFBs.

One of the intrinsic characteristics of AORFBs lies in the constitutive reduced stability voltage window: the theoretical electrochemical potential of H_2O electrolysis is usually 1.23 V, so the voltage in an AORFB cell is kept below such value to avoid electrolysis of water, thus limiting the overall stack's voltage.

1.5.1 Electrochemical considerations about AORFBs

Regarding other electrochemical parameters, some considerations are here presented, to highlight the main parameters impacting energy density and power density.

In RFBs, the energy density is determined by ELYs' concentration of active molecules, and by the voltage value that each cell can produce.On the other hand, power density is a very complex parameter: together with active species' concentrations and voltage values, it is also affected by the species' solubility and cells' kinetics.

At high currents, all RFBs present limitations of redox mediators in ELYs and severe, resulting in reduced power and energy density [29]. Research works of the last years has verified a higher polarization at high current density values. [28], where the main involved losses affect activation and concentration losses.

Reaction kinetics are mostly depending on redox reaction's potential, reversibility, and kinetics. Reaction kinetics are assessed with electron transfer rate constant (k_0). Higher k_0 indicates a faster reaction, while enabling a higher current density without raising overpotentials [29]. Some methods typically used to determine k_0 are: cyclic voltammetry and linear sweep voltammetry.

With respect to VRFBs, AORFBs show higher, liquid-enhanced electronic conductivity and ion mobility, currently providing relatively better performances at high power applications [29].

As concerning the cell voltage, if the active species' concentration is higher, it enhances higher energy as well as power performances, maximizing the voltage difference between anolyte and catholyte (thus increasing the cell voltage), but with both potential values within the solvent's electrochemical stability window. However, organic molecules structure can be tuned to have specific functioning groups to bring the highest potential window. It is possible to get higher cell voltage with different mediators for both catholyte and anolyte [29]. This feature, combined with faster kinetics reactions of organic molecules, opens the path to a higher power density.

Concerning the operating conditions, the pH significantly affects the stack components' internal resistances. Electrochemical stability voltage window can be regulated by adjusting ELYs' pH values. Although, at higher voltages levels, there is an increase of side reactions, causing a reduction of the pH. This leads to electrochemical stability problems, therefore in AORFBs it is essential to monitor the pH value.

Usual RFBs with metallic active species involve highly acid solutions, in order to keep high solubility of the active molecules. On the other hand, generally AORFBs do not involve acid solutions. For instance, in this work's study a highly basic pH condition has been kept, due to the chemical composition of very specific molecules developed by the technology providers who realized the AORFB devices examined in this work. In order to have a stable solubility, these organic molecules need high alkaline conditions conditions.

A higher charges' concentration increases energy density and enhances max current density, avoiding the risk of reactants depletion and/or voltage losses, thus allowing higher power density as well.

Here, AORFBs active species potential emerges: active molecules enable the increase of charge concentration by modifying the functional groups and structure of the organic species to improve the solubility and the quantity of storable electrons. Naturally, a compromise between mediators' electrochemical stability and high kinetic features has to be held in account.

Other operating conditions, such as flow rate and temperatures are crucial as well. High temperature improves kinetics and increases power performance, but redox species' instability issues might occurr, although with lower entity with respect to VRFBs.

To summarize, the use of organic active molecules has become a central research focus due to their lower cost, high properties' "tunability" and ease of customization of key properties, like solubility, redox potential, and kinetics, by changing organic functional groups and or structure. Obviously, the modification of redox species should compromise between stability and redox potential.

1.5.2 AORFBs' innovative aspects and potential

AORFBs' main goal consists of finding cheap and more procurable raw materials, with high solubility tailored organic molecules for aqueous electrolytes as the main solution to reduce RFBs' overall costs. [35]. Additionally, organic molecules result in less toxic and environmentally friendlier materials, providing a more sustainable alternative.

One of the current biggest challenges for AORFBs lies in the degradation phenomena affecting both the electroactive species and the cell components. The first type involves crossover of active molecules and side reactions, while cell materials undergoing degradation are electrodes, plates and the separator. All these factors lead to higher AORFB degradation with respect to VRFBs, and AORFBs show an average degradation of 1% during each year, thus affecting the performance of the organic technology. Plus, further aging is most likely to be recorded with higher cell voltages [28].

Nonetheless, the research of high performing molecules is currently undertaken, with competitive results expected in the upcoming five years. In the recent years, the majority of academic and research works have been focused on single cell examinations. Although their contribution on highlighting RFB technology' s important functioning principles, single-cell studies provide a very limited perspective on the practical operations functioning and behavior of full-scale redox devices.

The lack of experience about RFBs' application for complete devices can be filled only with dedicated studies on complete AORFB systems. Engineering considerations applied on real-size devices is crucial to explore and highlight this technology's features and actual performance, and proceed towards these devices' industrialization scale-up and commercial development. However, some present specific AORFBs molecules and devices are already showing interesting commercial solutions, with available systems offering truly promising performances.

In the next chapters, the performance investigation of an AORFB system has been deeply investigated, analyzing the operational behavior and practical results of a prototypal AORFB device. Moreover, economic considerations have been evaluated, to contextualize these systems' present possibilities.

Chapter 2

Methodology

2.1 Experimental setup

2.1.1 Laboratory Environment

This work's experimental campaign has been conducted in the Officine Edison laboratory, located at the ground floor of the Energy Center, which is part of the Politecnico di Torino campus in Turin.

The tested AORFB battery was installed and commissioned by the technology developers; the experimental setup and all testing procedures have been discussed and shared with the technology provider, in order to ensure safe operations and reliable measurements acquisition.

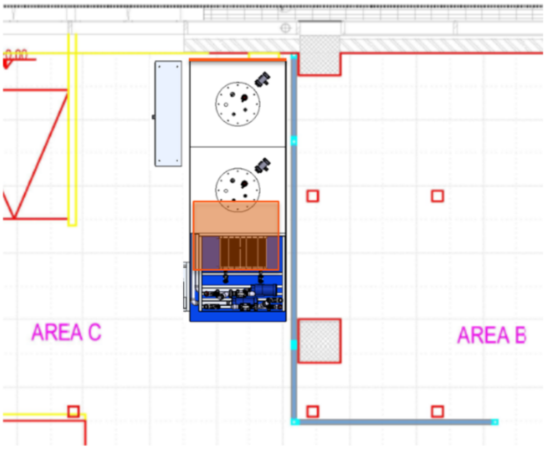

Figure 2.1: Plan view of the AORFB device in the Officine Edison laboratory

The AORFB test station is constituted by the tested storage system (battery and electric switchboard) and its test bench, engineered by Edison, to monitor and control the battery operations. The test station is provided with different electric supplies, in order to supply the battery itself and the test bench components, with the following characteristics:

1. Battery' supply, with 63A and 400V.
2. Switchboard supply, with 32A and 400V.
3. Switchboard auxiliaries, with 16 A and 400 V.

To simulate different charging and discharging conditions, the test bench includes an electronic load and a DC power supply with a dedicated three-phase inverter, connected in parallel both with the battery and the laboratory grid. The side emergency button allows to switch off the test station electric supplies, interrupting any connection between the battery and the workplace, to ensure safety in case of emergency.

The general supply selector is located on the battery's switchboard side: when the switch is on "1" position, the device is electrically connected.

The battery system consists of: the electrochemical cells unit, two tanks for the electrolytes, the Balance-of-Plant (pumps, piping, instrumentation and battery management devices) and the electric switchboard with the storage control logics, the inverter, and the interface with the external three-phase grid. While being the interface with the external grid, the electric panel is the operational center for all the battery's management operations for all electric, communication and control aspects.

The test bench hosts the control computer, to manage input and output data from interactions with the battery, and the devices for the generation and consumption profiles. The generation profiles are simulated by a three-phase DC power supply, provided with a FV inverter; the consumption profiles are produced by a three-phase electronic load. Both devices are directly involved during all the battery's experimental tests.

The laboratory is also provided with low pressure inert gas connections, in case any laboratory device would need some specific pressure values.

Since the battery works with liquid electrolytes solutions, the hydrogen production risk has been taken into account with a dedicated risk assessment with the supplier. However, this eventuality is always prevented, since the operative cell voltage is lower than water's electrolysis potential of 1.23 V.

The system is also provided with all security protections, ensuring the battery's proper functioning and the operators' safety. In particular, as further protection against possible electrolytes' leakages, the whole storage system is located within a containment basin, and it's surrounded by a perimetral protective screening.

The following part depicts the devices and software used during the experimental

Figure 2.2: Switchboard workplace, interface with the AORFB. Here, the electronic load is located, as well as the computer to interface with the battery device and the general supply selector.

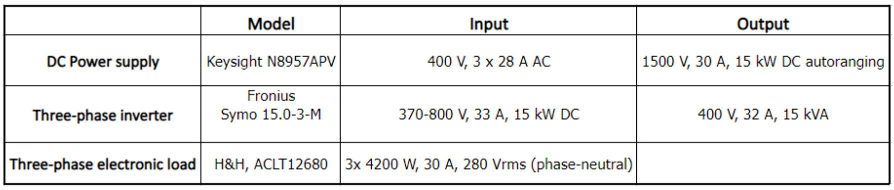

	Model	Input	Output
DC Power supply	Keysight N8957APV	400 V, 3 x 28 A AC	1500 V, 30 A, 15 kW DC autoranging
Three-phase inverter	Fronius Symo 15.0-3-M	370-800 V, 33 A, 15 kW DC	400 V, 32 A, 15 kVA
Three-phase electronic load	H&H, ACLT12680	3x 4200 W, 30 A, 280 Vrms (phase-neutral)	

Figure 2.3: Parameters of the electronic three-phase and generator load

campaign, to deeply examine the system's operational behavior and evaluate the technology's performance.

2.1.2 Battery system and software's technical specifications

Battery specifications

The electrochemical unit consists of 3 stacks electrically and hydraulically connected in parallel. Each stack contains 55 cells, which are electrically connected in series using bipolar plates.

Figure 2.4: AORFB's prototype device and interface workplace, shown during the battery installation phase.

This stacking configuration, showed in 2.6, will provide the level of voltage and power necessary for the power converters' proper operation conditions.

The battery's 55 cells connected in series per each stack ensure the battery device's main parameters, indicated in figure 2.7.

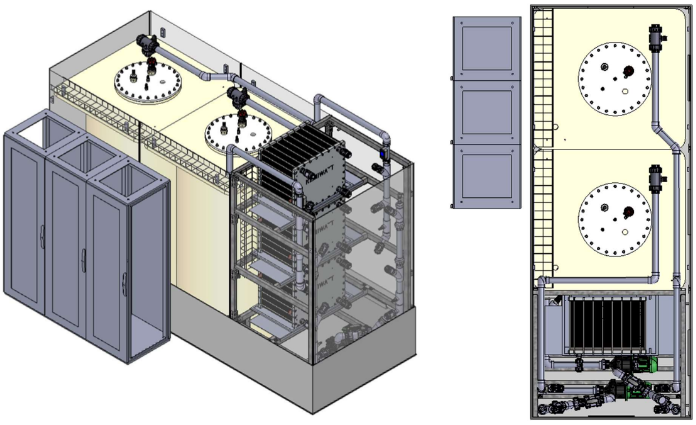

Figure 2.5: Battery device's visual rendering, given by the battery provider.

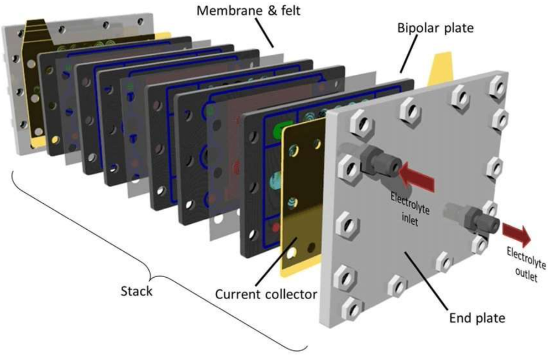

Figure 2.6: Battery's stack components view, given by the battery provider. The electrolytes'inlet and outles are shown, as well as the disposition of the cells' membranes, bipolar plates and felts within the stack, with the current collectors on the sides.

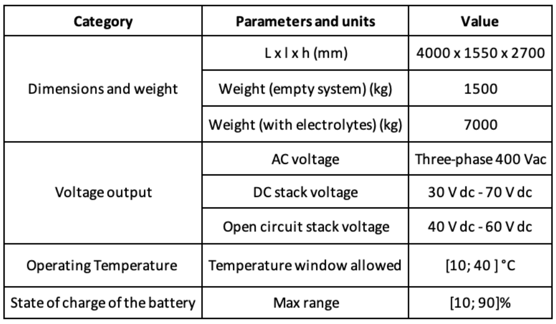

Category	Parameters and units	Value
Dimensions and weight	L x l x h (mm)	4000 x 1550 x 2700
	Weight (empty system) (kg)	1500
	Weight (with electrolytes) (kg)	7000
Voltage output	AC voltage	Three-phase 400 Vac
	DC stack voltage	30 V dc - 70 V dc
	Open circuit stack voltage	40 V dc - 60 V dc
Operating Temperature	Temperature window allowed	[10; 40] °C
State of charge of the battery	Max range	[10; 90]%

Figure 2.7: Battery device's parameters, given by the technology provider. In here, the operational limits of voltage, temperature and state of charge are shown.

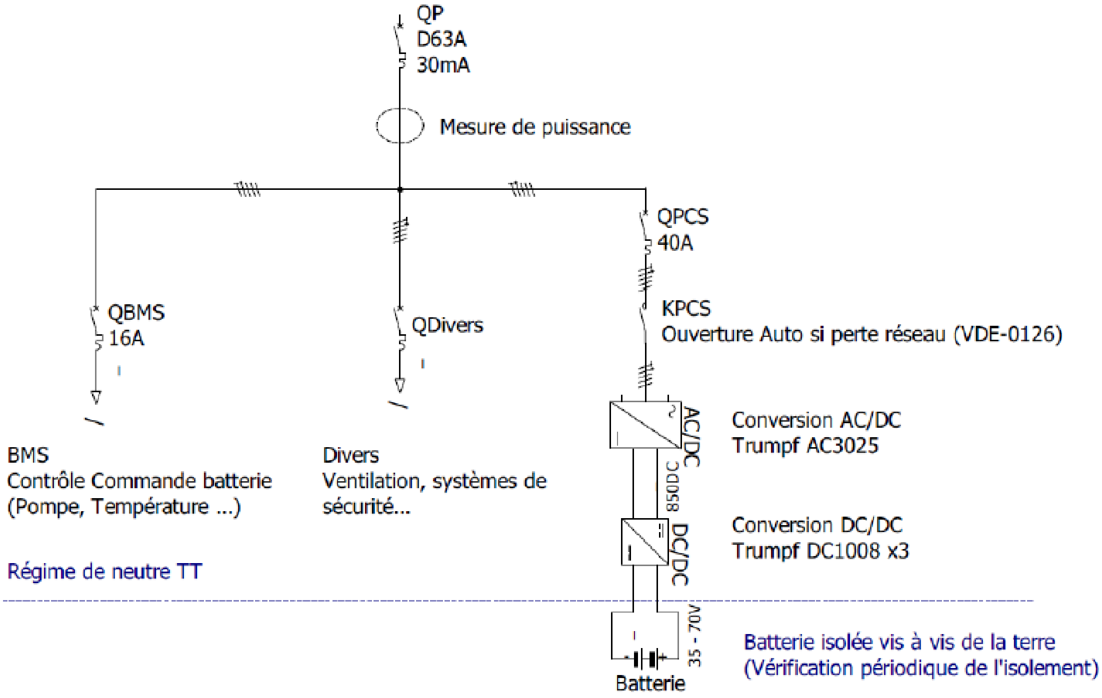

Figure 2.8: AORFB system's electric scheme, shared by the technology provider.

The system operation during charge and discharge follows all the steps of AORFBs

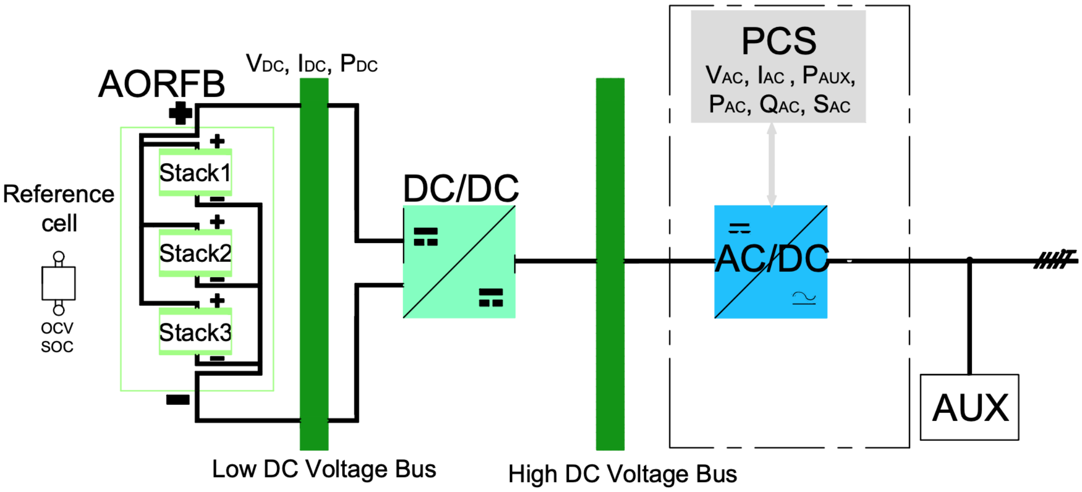

Figure 2.9: AORFB's electric blocks connections, where the three stacks are shown, electrically connected in parallel. The DC/DC converter is necessary to increase the battery's output low voltage. The power conversion system (PCS) not only regulates the AC/DC converter, while PMS is the interface controls PCS and BMS, and applies current and power limitations.

technology introduced in Chapter 1.
From the tanks, kept at a pressure level indicated by the technology providers, the pumps constantly inject the electrolytes within the stacks' cells, where reversible redox reactions occur. The liquid solutions of catholyte and anolyte advance in the stack's flow channels in counter-flow mode (as can be seen from the figure 2.6), to reduce the overall pressure losses within the stack and, at the same time, to assure the best flow conditions during operative conditions.
When all redox reactions are concluded and the operation ends, the electrolytes are pumped back into the tanks, where they are stored until a new energy application is undertaken.

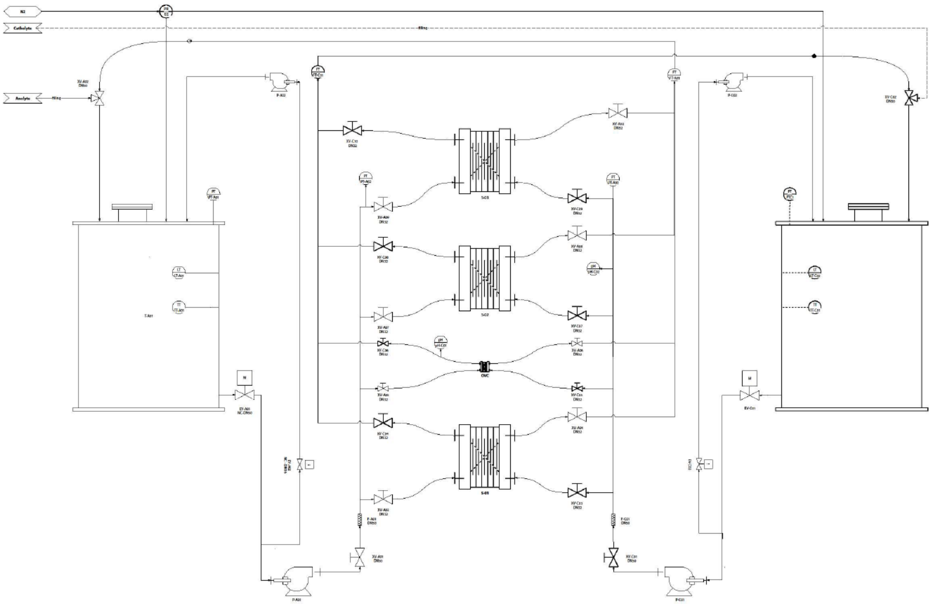

Figure 2.10: AORFB system's hydraulic scheme, shared by the technology provider. The many pressure sensors and valves are illustrated, indicating the main monitored pressure values in the cells, pipes, and tanks.

A separated reference cell, installed outside the stack, is fed with the same electrolytes pumped into the main stacks and kept disconnected from any electric load. In this way, the reference cell measures the Open-Circuit Voltage, which depends mainly on active species concentration and temperature and is not affected by external circuit resistance.

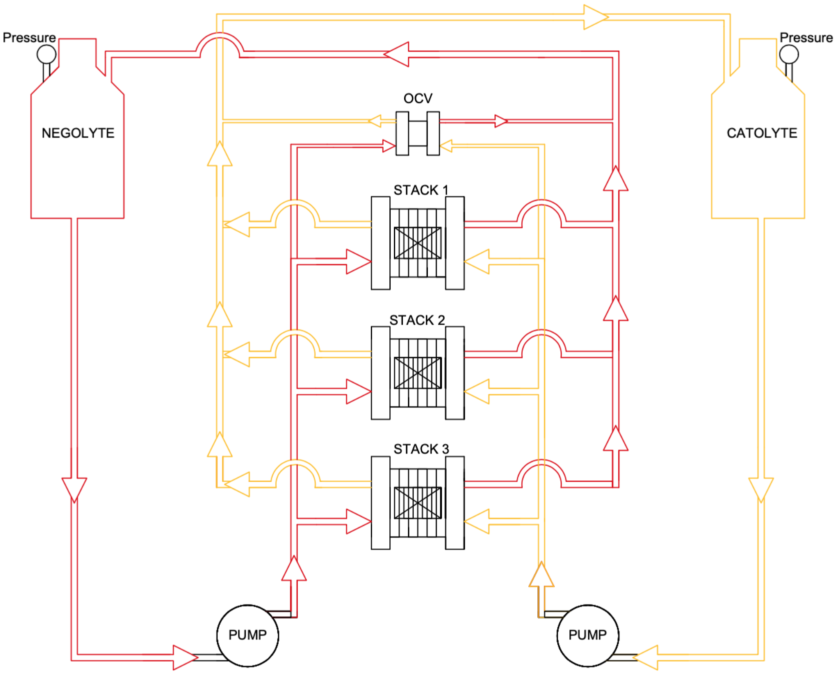

Figure 2.11: AutoCAD's rendering of the AORFB hydraulic connections, depicting the counter-flow flowing of the electrolytes. The main pressure valves on the tanks, determining the controlling setting's value, are illustrated here.

AORFB device control software

In all redox-flow systems, the reference cell is used by the Battery Management System (BMS) to estimate the real-time battery state of charge (SOC), through a proprietary algorithm. Since the SOC is obtained from calculation methods rather than directly measured, for the following experiments both empirical values of OCV and values of SOC have been checked, to provide coherent and representative measures and results.

In this work, the adopted sign convention is the one for generators: negative parameters indicate elements adsorbed by the battery (including current and/or power in charge operations, as well as auxiliaries' consumption), while positive values indicate elements produced by the device (as current and/or power in discharge operations).

The Battery Management System (BMS) is the battery control unit, responsible for the actions listed below.

1. All measurement at cell/stack level.

2. Electrolytes' conditions monitoring.

3. Pumps and valves control.
4. SOC estimation.
5. All safety controls.

The Power Conversion System (PCS) is the element controlling the power converters. To interface with the external grid and, in general, to AC loads, a DC/AC converter is embedded in the storage. It is regulated by the Power Management System (PMS), which also controls and applies limitations to power and current flow. At the same time, PMS controls both PCS and BMS. As shown in the electric system's scheme, V_{dc}, I_{dc}, and P_{dc} are measured at the low-tension bus. Since AORFBs work at low voltage levels, to adapt the voltage exiting the battery to the external load's voltage, a DC/DC converter is installed to increase the DC voltage. Energy storage auxiliaries, mainly the pumps, are connected on the inverter mains side, and independently measured by the PMS.

The PMS coordinates the lower management and control levels of the storage system, including the BMS; in addition, the PMS is also the main interface with the end-user's management and control system. Relevant measures, alarms and control variables are managed by the PMS, which makes them available for the user on the Modbus/TCP IP protocol.

The interface to interact with the battery device and insert input values is provided by the Front Panel of the graphical programming development environment LabVIEW (Laboratory Virtual instrument Engineering Workbench). The graphical approach of LabVIEW's programming is based on Virtual Instruments, interconnected blocks and icons containing functions, applications, subroutines or generic commands.

The Front Panel shows all the controls, indicators and inputs that the user can interact with. User's inputs are executed by the code present in the Block Diagram (here not shown). LabVIEW's functioning principle follows a dataflow model, where the order of data determines the program's execution. The numerous functions and nodes are executed when all input values are inserted, giving as outputs the programmed calculations and operations (which then become input values of the following nodes, and so on). The entirety of LabVIEW's program, blocks and structure used in this work had been defined and implemented before this work's beginning, and the Front Panel interface has only been used exclusively to interact with the AORFB device examined in this work.

LabVIEW also allows interaction with external hardware elements, such as a data acquisition system accessed through a Navicat software, linked to Edison's database to collect the experimental measured data.

As first step, the desired settings have to be inserted in the Front Panel. Together with the electronic load and storage addresses (necessary for these devices' electronic configuration in the laboratory), the main settings are:

1. SOC lower and upper limits, here with the set desired values of 10% and 90% respectively.
2. Logging period, corresponding to the period when each sample is memorized and saved on the database. While the acquisition period is two seconds per each element, the logging period for the experimental campaign in this work has been set to 6 seconds for short tests, and 1 minutes or 20 seconds for longer ones.

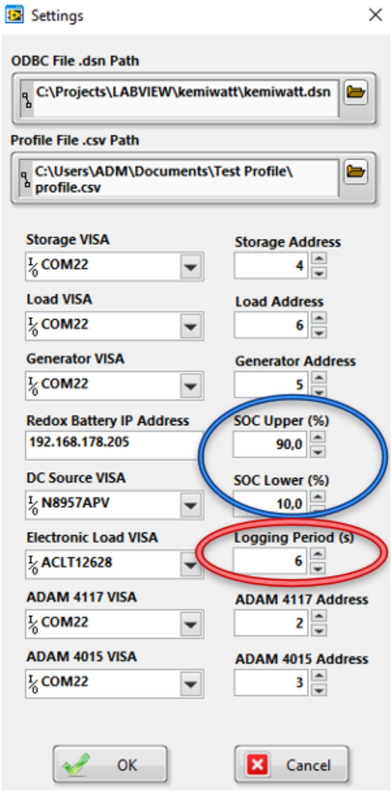

Settings

ODBC File .dsn Path: C:\Projects\LABVIEW\kemiwatt\kemiwatt.dsn

Profile File .csv Path: C:\Users\ADM\Documents\Test Profile\profile.csv

Storage VISA: COM22
Storage Address: 4
Load VISA: COM22
Load Address: 6
Generator VISA: COM22
Generator Address: 5
Redox Battery IP Address: 192.168.178.205
SOC Upper (%): 90,0
DC Source VISA: N8957APV
SOC Lower (%): 10,0
Electronic Load VISA: ACLT12628
Logging Period (s): 6
ADAM 4117 VISA: COM22
ADAM 4117 Address: 2
ADAM 4015 VISA: COM22
ADAM 4015 Address: 3

Figure 2.12: LabVIEW's adopted settings. The most crucial parameters are represented by the upper and lower SOC limits. The battery's cycles do not start until SOC lies within the indicated limits. On the other hand, the logging period indicates the database acquisition time for the experimental measures.

For the conducted experimental tests, the battery inputs, inserted and modifiable in LabVIEW, are time steps duration in seconds ("Duration (s)") and power, expressed in Watt ("P_{storage}"). Negative power inputs activates the charging phase, while positive power values perform a discharging operation.

These inputs, inserted in the "Profile" window, allow the configuration of the charge

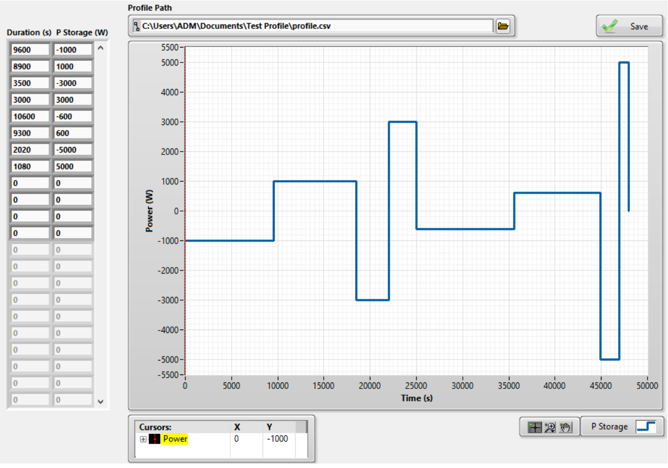

Profile Path

C:\Users\ADM\Documents\Test Profile\profile.csv

Duration (s)	P Storage (W)
9600	-1000
8900	1000
3500	-3000
3000	3000
10600	-600
9300	600
2020	-5000
1080	5000
0	0
0	0
0	0
0	0
0	0
0	0
0	0
0	0
0	0
0	0
0	0
0	0
0	0
0	0

Cursors:	X	Y
Power	0	-1000

Figure 2.13: LabVIEW's front panel example profile. The power values are inserted here, where negative positive and inputs apply a cycle of charge and discharge, respectively. Each cycle's duration is set via the respective time input.

and discharge profile that the battery will perform during the test. Once the battery profile is set and configured, the system operation is activated with the "Acquisition Start" command.

During the battery's operation, the main parameters that can be monitored via LabVIEW are:

1. System's DC values of current, voltage, power, and auxiliary consumption, all controlled by the PMS.
2. System's AC values of current voltage, giving active, reactive and apparent values, comprehensive of auxiliary consumptions.
3. Single cell's minimum and maximum voltage, OCV and SOC values, all controlled by the BMS.
4. Tank's pressure values [bar], controlled by the BMS.
5. Electrolytes' flow rate, in [L/min], and stack temperatures [°C], all controlled by the BMS.
6. Electronic load's values of current voltage, and values of power levels for DC and AC (the latter, giving active, reactive and apparent values).

The figure 2.14 shows a segment of an operating cycle during an experimental test, as well as DC current and voltage.

Once the cycle profile is configured through the power and duration inputs, the

Storage Power (W) 2000

Time Stamp 30/03/2023 16:44:31.503

SOC (%) 19.0

Acquiring and Logging...

Figure 2.14: LabVIEW's front panel display. The stacks' profile of current and voltage are shown on the left, as well as the real-time measured SOC level. The bottom-right side shows the power profiles of the battery devices, of the auxiliary consumption and of the overall system. The values of electrolytes' temperature and pressure within the cells are displayed as well, together with some sensors to detect eventual faults in the PCS or BMS.

"Acquisition Start" command allows the cycle's beginning, abut only after the pressure value within the tanks is checked. As a safety measure, the battery's electrolyte within the tanks is kept at a set pressure value.

Once both tanks' pressure constraints have been fulfilled, the pumps start injecting the electrolytes through the hydraulic circuit displayed in 2.11. In the stacks, each electrolyte enters at the bottom and exits at the top. As can be seen in advancing in counter-flow direction with respect to the electrolyte with opposing charges, then the two fluids enter their respective tank.

When the battery has to be disconnected, i.e. for long inactivity periods, the "Battery Stop" mode is selected.

2.2 Techno-economic model

2.2.1 Cost estimation approach

Chosen cost invoices

As introduced in Chapter 1, AORFBs' technological potential is currently being examined all around the world. Unfortunately, while numerous studies have been performed on cell-scale, the current lack of literature on techno-economic considerations for AORFB battery-scale devices prevents a detailed examination of the practical feasibility of AORFB devices.

In this work, a techno-economic analysis has been undertaken, to provide a perspective on the costs involved to this technology's realization. This analysis also included the yearly degradation incurring in AORFB performance, to describe a characteristic currently present in this technology, and to provide realistic and representative economic values.

The techno-economic considerations of this work are inspired by the work on RFB developed by the Pacific Northwest National Laboratory (PNNL) [32], from which the values for cost invoices have been used as reference. Their approach exploits documented costs invoices obtained from numerous large-scale industrial providers, to get a comprehensive dataset of the benchmark costs to be approached to realize a RFB system for different sizes [36].

In this work, a techno-economic model has been implemented, selecting the most suitable cost invoices and adapting them for AORFBs' technology. Most of the invoices values' trends of the chosen cost invoices have been interpolated with respect to the varying nominal power, and with cost invoices of electrolyte and tanks also depending on duration discharge. The techno-economic model's inputs consist of:

1. P_n: AORFB's nominal power, between 10 kW and 100 MW.
2. t_n: nominal discharge duration, between 2 and 100 hours.
3. DOD: depth of discharge.
4. RTE: roundtrip efficiency

This techno-economic evaluation calculates the following outputs: capital expenditure (Capex), operational expenditures (Opex), battery's produced energy, and levelized cost of storage (LCOS). The latter represents the price to be assigned to a unit of energy produced by a storage device, in order to cover all the storage necessary costs (including financial costs, replacement, etc) and to repay the whole investment. Moreover, LCOS is a key parameter to compare capital and operating costs of numerous storage technologies with different characteristics, with respect to the the devices' effective cycle performances throughout their total operational life. Along with more detailed considerations, LCOS is a key indicator to realistically represent the actual feasibility of a storage project.

2.2.2 Costs invoices breakdown

The first step in the pursue of total Capex calculations involves the selection of the necessary costs. The chosen costs values and relative sub-voices, provided by [32] and accounted in this work, are the following:

1. Storage block(SB) [kW/h]: stack (bipolar plates, bipolar, carbon felt, PVC frame, membrane separator), tanks and ELY costs.
2. Balance of system (BOS) [kW/h] (pumps and valves)
3. Electronics [kW/h] (Power conversion system)
4. System Integration costs [kW/h]
5. CC [kW/h]: control and communication sensors and devices.

The specific costs listed above are expressed either with respect to the storage energy capacity or in terms of their nominal power. These benchmark costs for 4 hours are provided by [32] and [37], for power sizes of 1, 10 and 100 MW.
The costs expressed as function of energy capacity have power-depending trends. From reference given data in [32], these costs' trends have been extrapolated to provide the cost values of SB, BOS and System Integration for intermediate P_n inputs values between 10 kW and 100 MW.

Electrolyte cost's calculation

In this work, the main difference on the selected cost invoices, with respect to VRFB reference values, involves the SB costs, varying for a more economically convenient electrolyte (ELY) cost, way cheaper with respect to the vanadium-based technology. The fundamental step of this work consisted in obtaining the electrolyte cost for AORFBs.
In [32], the cost invoices values are given, while the percentages of such reference cost invoices are provided by [37], giving more detail on the main components and the weight they hold in the total cost of an AORFB device. For VRFB technology, the average membrane separator accounts for more than 25% of the initial capital investment. But as shown in [37], the predominant cost factor is represented by the electrolyte cost, showing a direct evidence of what anticipated in the introduction

chapter.

The exploited approach calculates the individual specific cost values of VRFB in $[/kWh]$ from the percentages provided in [37] applied to the sum of SB, BOS and Electronics values from [32]. Therefore, the calculated cost sub-voices are obtained, allowing to get the VRFB ELY cost sub-voiceas well. Except for the VRFB electrolyte, these sub-voices' values will be used for AORFB as well, since (as anticipated in this section) the main cost invoice difference lies in the electrolyte. Then, knowing the sum of the overall costs for AORFB from the technology providers, the sub-voices' new percentages for organic batteries are found, and by subtraction the new organic electrolyte cost is obtained.

The calculating steps are illustrated hereafter. This methodology calculates the individual specific cost values of VRFB in [$/kWh] from the percentages provided in [37], applied to the overall sum of SB, BOS and Electronics. Hence, the specific VRFB electrolyte cost and all SB's sub-voices (bipolar plates, carbon felt, PVC frame, membrane, tanks and ELY) are obtained. For VRFB, the provided sum consists of VRFB ELY cost and 8 sub-cost invoices: Electronics; bipolar plates, felt, PVC frame, separator, and tanks, forming SB; pumps and "other" (mailny including valves and heat exchange devices), forming BOS.

From the PNNL report reference [32], the sum of ELY cost and these 8 sub-invoices is known, in $[\$/kWh]$, for $P_n = 1MW$ and $t_n = 4h$. And from [37], the percentages of each of the above-mentioned cost sub-voices are displayed.

By applying the percentages to the overall sum, the eight sub-voices' values are obtained, in $[\$/kWh]$. The values expressed in $\$/kWh$ have been simply multiplied for 4h, to get coherent units of measurement). The VRFB ELY cost's numerical values is also obtained, equal to circa $155[\$/kWh]$, reflecting the usual average values for vanadium-based electrolytes.

The calculation for ELY cost of AORFB is now undertaken, this time with

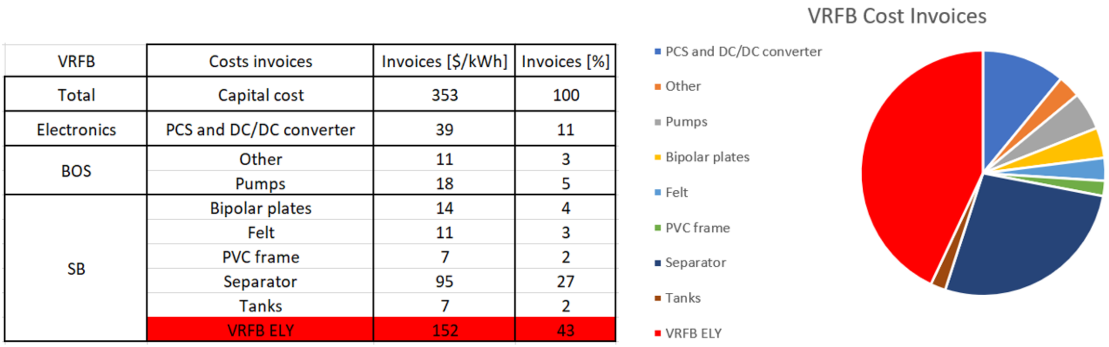

VRFB	Costs invoices	Invoices [$/kWh]	Invoices [%]
Total	Capital cost	353	100
Electronics	PCS and DC/DC converter	39	11
BOS	Other	11	3
	Pumps	18	5
SB	Bipolar plates	14	4
	Felt	11	3
	PVC frame	7	2
	Separator	95	27
	Tanks	7	2
	VRFB ELY	152	43

Figure 2.15: VRFB costs percentages and invoices values. The percentages indicated in [37] are applied to the overall costs provided in [32], obtaining the specific values of the individual cost voices, especially the electrolyte's value.

respect to a cost summation equal to the initial investment capital cost $CF_{0,\text{base}}$ value. This AORFB's sum value, expressed in $[\$/kWh]$, has been shared by the technology providers who realized the AORFB device experimentally examined in this work. By applying the cost invoices' percentages to the overall cost values, the new organic electrolyte cost has been obtained.

$CF_{0,\text{base}}$ consists of the same 8 VRFB cost sub-voices plus the values System Integration and CC costs. Assuming the same VRFB 8 sub-voices values, and adopting the same System Integration and CC costs for vanadium-based devices, the new costs percentages for AORFB are evaluated. By subtraction, we get the new AORFB's electrolyte cost, falling in the range between 30 and 40 $[\$/kWh]$. With this newfound electrolyte's value, the new techno-economic model implements the AORFB's SB cost equal to the relative reference cost invoice minus the difference between vanadium's electrolyte cost and the new-found organic electrolyte cost. The new SB value for organic batteries is thus obtained.

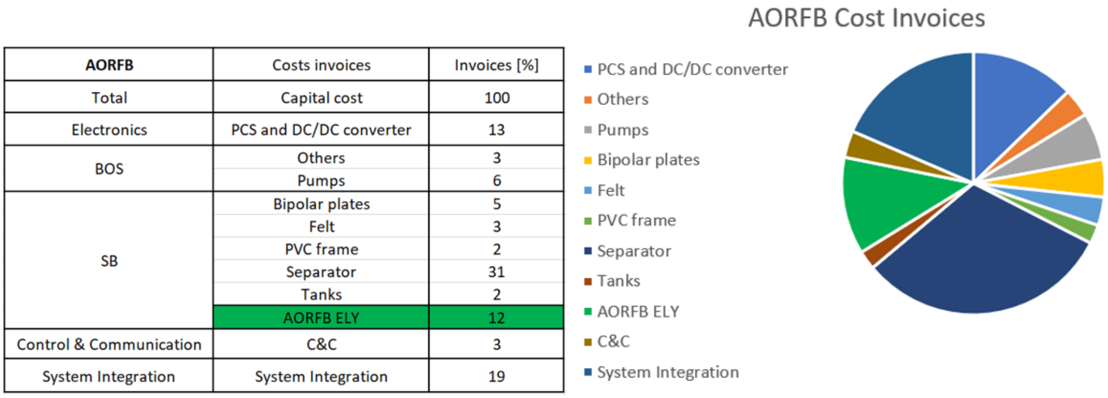

AORFB	Costs invoices	Invoices [%]
Total	Capital cost	100
Electronics	PCS and DC/DC converter	13
BOS	Others	3
	Pumps	6
SB	Bipolar plates	5
	Felt	3
	PVC frame	2
	Separator	31
	Tanks	2
	AORFB ELY	12
Control & Communication	C&C	3
System Integration	System Integration	19

Figure 2.16: AORFB costs percentages. The overall costs sum value has been hsared by the technology providers, while the same cost values for the same 8 sub-voices used for VRFB have been kept constant. Then, the individual percentages have been obtained, and used to calculate the organic electrolyte value. The new organic electrolyte is circa 70% lower than the average one for vanadium batteries, thus reducing this component's impact on the battery's overall expenses.

$$\Delta ELY = ELY_{\text{VRFB}} - ELY_{\text{AORFB}} \tag{2.1}$$

$$SB_{\text{AORFB}} = SB_{\text{VRFB}} - \Delta ELY \tag{2.2}$$

The other considered cost values (BOS, Electronics, System Integration, and CC) are kept the same even for AORFB, with a variation with P_n.

Trends' evaluation with MatLab and Python

Before performing costs calculations, the trends for SB, BOS and System Integration costs are evaluated, to get these costs' extrapolated values depending on the intermediate power input. To get the power-dependent trends of these costs, MatLab's "Curve fitting") tool (cftool) has been used. From known costs data, this tool allows to get the best-fitting curve. The model's chosen equation to represent SB, BOS and System Integration is the following:

$$z = a * x^b \tag{2.3}$$

The approach consists of performing a curve-fitting of SB, BOS and System Integration costs, depending on numerous values of P_n. With MatLab's cftool, it is possible to obtain:

1. Curves that better approximate these trends
2. Parameters' initial values, necessary for the trend evaluation.
3. Goodness of fit's parameters, to check trend's accuracy.

Plots from MatLab cftool allow to get the trends of SB, BOS and System Integration for different values of P_n, are displayed from curve fitting, as shown in the figure 2.17.

Cost evaluation for time and power dependance

Once the parameters and the equations from MatLab have been found, the fitting equation 2.3 is applied with a fitting Python code (illustrated, together with the whole techno-economic model's code, in Appendix B). Once the power-dependent trends have been calculated, the efective costs calculation can be performed.
Like the trends of BOS and System Integration, the SB trend evaluated so far is extrapolated from the reference costs, which are referred to benchmark values of 4 hours [37] (therefore named SB_4).
Expressing the overall cost for reference values referred to 4 hours, the initial investment expenditure $CF_{0,\text{base}}$ is obtained by the sum of the above-mentioned costs, with all values expressed in [\$/kWh]. On the pther hand, the costs expressed in \$/kW are divided by 4 hours, to get coherent units of measurement).

$$CF_{0,\text{base}}[\$/kWh] = SB_4 + BOS + Electronics + SystemIntegration + CC \tag{2.4}$$

Once $CF_{0,\text{base}}$ is obtained, pumps costs are evaluated by applying the respective reference percentages in [37], as indicated below:

$$Pumps = 5\% CF_{0,\text{base}} \tag{2.5}$$

Before evaluating the other cost invoices'values, some clarifications here are necessary. It is important to remember that, even keeping the stack's size constant and

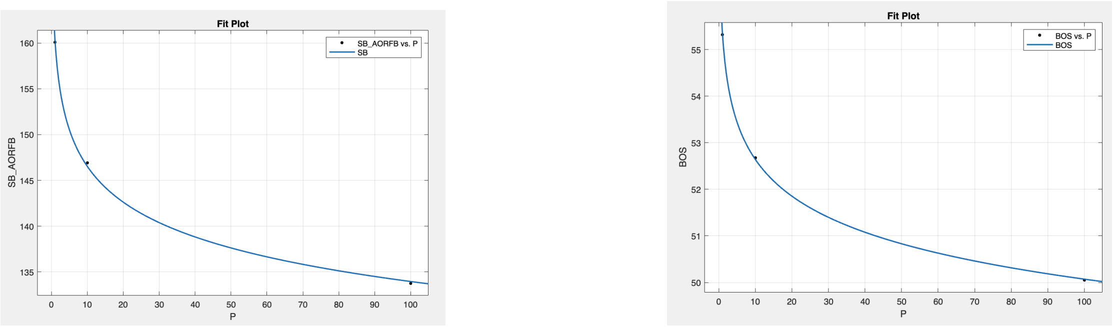

(a) SB trend from MatLab's cftool

(b) BOS trend from MatLab's cftool

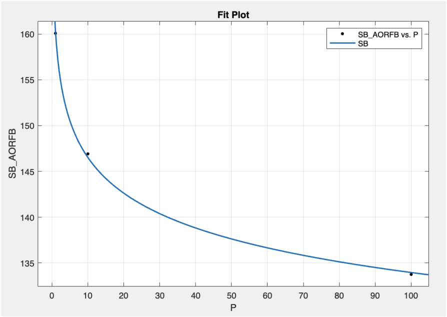

(c) System Integration trend from MatLab's cftool

Figure 2.17: Trends of SB, BOS and System Integration invoices. The displayed graphs, obtained from MatLab's cftool, visually show the accuracy of the adopted formulae to represent these trends, to get the invoices' values for any power input values between 10 kW and 100 MW.

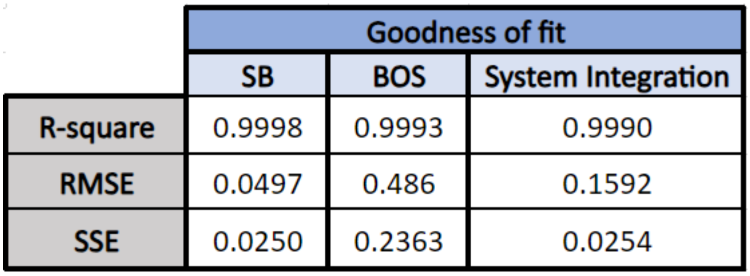

	Goodness of fit		
	SB	BOS	System Integration
R-square	0.9998	0.9993	0.9990
RMSE	0.0497	0.486	0.1592
SSE	0.0250	0.2363	0.0254

Figure 2.18: Goodness of fit coefficients of cftool's trends. All the values of R-square are very close to 1, proving the trend's high accuracy. The RMSE (Root Mean Square Error) low values indicate a low discrepancy between the reference values and the ones of the trends'. Finally, SSE (Sum of Square Errors) low values express a low sum of squared residuals, and the consequent trends' validity.

operating at the expected nominal power P_n, to get more energy from AORFB it is possible to simply increase the quantity of electrolyte, depending on the needed or desired energy.

On the other hand, stack costs are predominantly dependent on the power size and stack's related costs of AORFB, like the pump costs. This constitutes the main flexibility of AORFB systems.

Therefore, ELY and Tanks costs vary with the application nominal discharge duration t_n and the desired energy output. The volume of ELY and consequent tanks' dimension are linearly dependent with t_n, which influences the AORFB device's design.

Depending on the application and the desired energy, the volume of ELY and consequent tanks' dimension are linearly dependent with the nominal duration of discharge t_n, which influences the AORFB application and design. Even keeping the stack's size constant, to get more energy from AORFB it is possible to simply increase the quantity of ELY based on the needed or desired energy.

On the other hand, stack costs are predominantly dependent on the power size of AORFB. This constitutes the main flexibility of AORFB systems.

However, since the costs for stack, electrolyte and tanks are given from the reference [32] as percentages of $CF_{0,\text{base}}$, it's necessary to get ELY's and tanks' unitary cost values (in $\$/kWh$) for reference 4 hours values, get the stack costs, and then "adapt" ELY and tanks effective costs to the actual duration. Therefore, "nominal" values for tanks (Tanks4)[$\$/kWh$] and ELY ($ELY_4$) are introduced , both expressed as [$\$/kWh$], where the subscript "4" namely indicates that these are the reference costs' values for 4 hours.

$Tanks_4$ is calculated right after the trends' evaluations,given by the reference percentage of 2% applied to $CF_{0,\text{base}}$ [37]. On the other hand, (ELY_4) simply indicates the value of organic ELY cost calculated earlier.

Then, by subtracting $Tanks_4$ and ELY_4 from the initial SB value, called SB_4, the stack cost is determined (in [$\$/kWh$] as well).

Therefore, the following equations are implemented:

$$Tanks_4 = 2\% CF_{0,\text{base}} \tag{2.6}$$

$$Stack = SB_4 - ELY_4 - Tanks_4 \tag{2.7}$$

At this point, cost values in [\$] have to be obtained from the considered cost voices, which depend either on energy capacity or power size. In fact, Electronics and CC costs are expressed in [\$/kW] since they depend on power only, therefore, they're just multiplied by P_n.

On the other hand, among the costs depending on the energy capacity (SB, BOS and System Integration), only ELY and tanks, belonging to SB, truly depend on the nominal duration. From SB, to get effective costs in \$, ($Tanks_4$) and (ELY_4) values are multiplied by the input desired t_n.

At the same time, the stack value, BOS and System Integration are all multiplied by 4 hours, thus keeping the reference value upon which the reference costs are given in [32]. In the end, once the actual SB is calculated, the relative actual CF_0, expressed in [\$], is therefore obtained.
Finally, the replacement costs are evaluated as a mandatory expense at the 12th operation year, thus indicated as CF_{12}. The replacement cost consist of the sum of stack and the previously calculated pumps costs.

$$CF_{12}[\$] = Stack + Pumps \tag{2.8}$$

The adopted steps are the summarized here:

1. After trends' extrapolation, $CF_{0,\text{base}}$ and pump costs are calculated.
2. From $CF_{0,\text{base}}$ and SB_4: reference percentages are applied to get $Tanks_4$, and $Pumps$.
3. Evaluation of the energy costs depending on the discharge duration, i.e. ELY and Tanks.
4. Energy costs not depending on duration are calculated.
5. Power-dependent costs calculation.
6. Replacement costs evaluation (CF_{12}).

In figure 2.19, a comprehensive map of the calculations step is displayed.

Capex and Opex calculation

Accounting all the cost invoices described in the previous section, the calculations for Capex and Opex can be performed. Further details about economical parameters and their relative values are illustrated in the Appendix A.
Capex involves both the initial cost expenditure and the replacement cost at the 12th year, where the stack and the pumps have to be substituted.

$$Capex = \frac{\sum_{n=0}^{N} CF_n}{(1+d)^n} \tag{2.9}$$

$$Capex = CF_0 + \frac{CF_{12}}{(1+d)^{12}} \tag{2.10}$$

In these formulae and in the following ones, N indicates the project's years (here assumed 20 years), and d indicates the value of the real weighted average cost of

capital.
Next, Opex calculation is performed through the following expression:

$$Opex[\$] = 0.43\% CF_0 + 30\% \frac{Electronics}{N} \tag{2.11}$$

In the equation 2.11, the first term encapsulates the typical maintenance costs for RFBs, while the second term indicates an extraordinary maintenance for electronic components. It is performed once at the 12th year, but its cost is spread along the whole project life and considered as an Opex cost, rather than Capex.
After the quantification of the global expenditures, it is possible to proceed with the equation of the levelized cost of storage (LCOS) [38].

$$LCOS[\$/kWh] = \frac{Capex + Opex \cdot \sum_{n=0}^{N} \frac{1}{(1+r_b)^n} + \frac{p_e \cdot E_b}{RTE}}{E_b} \tag{2.12}$$

Where r_b is the rate of discount for batteries, p_e is the electricity cost to recharge the battery device, assumed equal to 175 €/MWh [39]; RTE indicates the AORFB's roundtrip efficiency, and E_b is the AORFB's globally discharged electricity, expressed as:

$$E_b[kWh] = c_b \cdot DOD \cdot RC \cdot \sum_{n=1}^{N} \frac{1 - DEG \cdot n}{(1 + r_b)^n} \tag{2.13}$$

Where c_b is the number of annual cycles completed by the battery and DOD is the depth of discharge. RC stands for the AORFB's rated capacity, while DEG is the annual percentage of degradation suffered by the battery. For AORFBs, the average yearly degradation accounts 1% of energy losses in the battery. With a maximum reference value of cycles per year set as c, m=365 [38], the effective annual cycles have been calculated with the following expression [32]:

$$c_b = c, m \cdot min\left(\frac{1}{DOD}, \frac{24}{CT + DT + 2 \cdot t_{\text{rest}}}\right) \tag{2.14}$$

Where DT and CT represent the battery's discharging and charging time respectively, while *rest* indicates the needed resting time to avoid an increase of temperature. While t_{rest} in vanadium batteries is considered equal to 30 minutes for discharges lasting less than 4 hours, as indicated in [32], in AORFBs there is no risk related to a temperature increase, therefore t_{rest} is assumed null in this work. The following equations quantify the discharging and charging time:

$$DT[h] = DOD \cdot RC \tag{2.15}$$

$$CT[h] = \frac{DT}{RTE} \tag{2.16}$$

As further addressed in the following section, the roundtrip efficiency value needs a specification. The RTE performance is one of the key parameters to ensure the economical feasibility of ESSs' feasibility and realization, as well as the expected operative performance desired from the storage device.

For current commercially available solutions, as well as the device tested in this work, AORFBs present RTE values of circa 50%. Nonetheless, according to the most realistic scenarios illustrated by the technology providers of the AORFB device experimentally tested here, efficiency values for AORFB are foreseen to reach 65% within the upcoming 5 years. This value is really close to more mature vanadium-based batteries, and reaching this efficiency for AORFBs is current objective and focus of countless research works.

Considering the reliability of the technology providers of the AORFB system studied in this work, the results displayed in Chapter 3 show a sensitivity analysis for different RTE values, and quantify the exact weight of such parameter in techno-economic calculations.

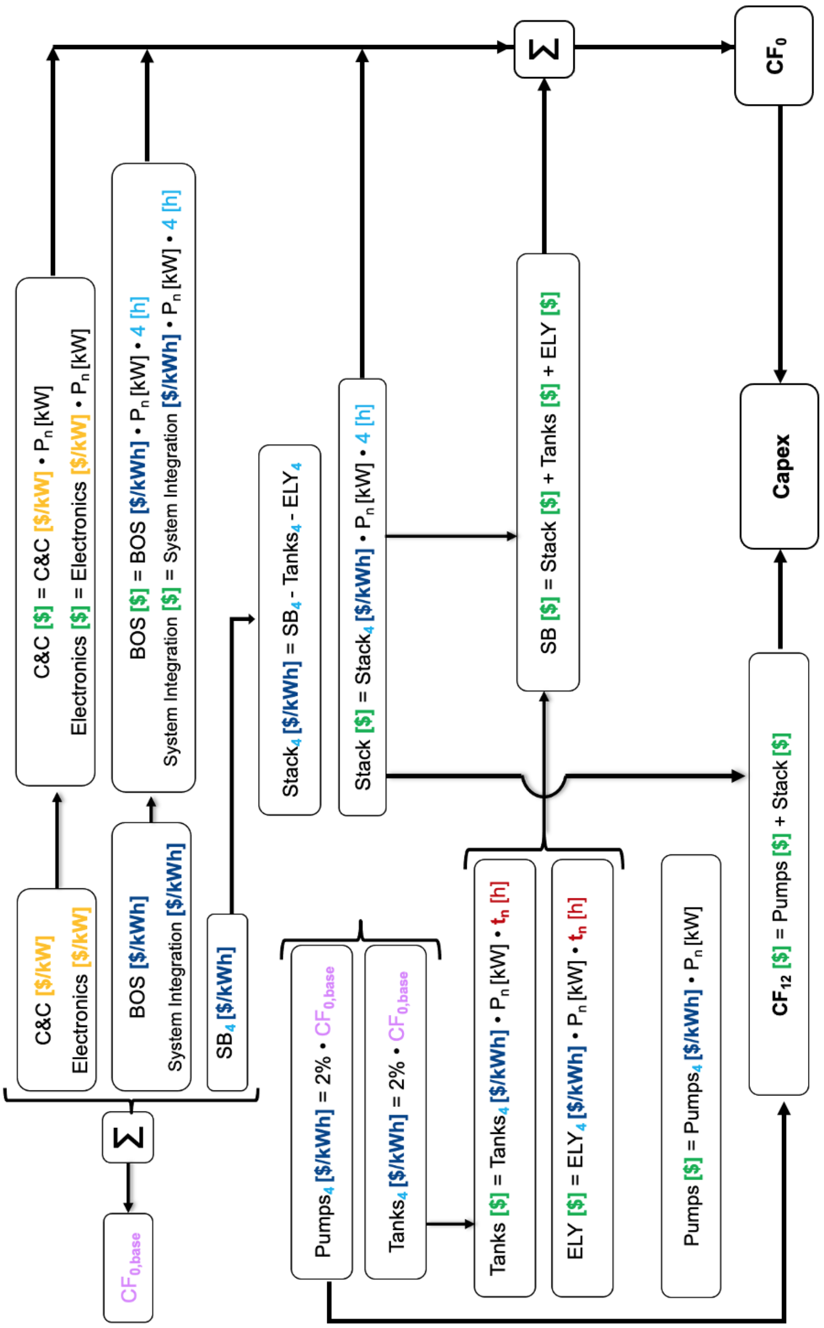

Figure 2.19: Conceptual map of the cost calculation steps. The cost related to power only are multiplied by P_n. Among the cost depending of energy capacity, System Integration and BOS values are the same as VRFB's four hours reference values from [32], since they don't vary with discharge duration tn. From SB, on the other hand, Tanks and electrolyte costs depend on the application duration and are multiplied for tn. Once all the costs are referred to monetary unit of measurement [$], the actual CF_0 and CF_{12} are obtained, and Capex can be calculated.

Chapter 3

Results and discussion

3.1 Experimental analysis

3.1.1 Performed tests typologies

The experimental campaign on the prototype analyzed in this work has been focused to show and validate the operational functioning of the AORFB system technology. The electrochemical direct current (DC) results evaluate the battery's chemical energy performance. On the other hand, the alternating current (AC) values are measured in correspondence of the DC/AC converter, and they consider the global performance of the whole system. AC values account for all necessary components for the battery complete functioning, including electrochemical performances integrated with the auxiliary power consumption (from pumping devices, PMS, BMS and PCS control devices, and occasional heating devices). While DC results depend on AORFB's electrochemical characteristics and performances only, AC values are strongly affected by the system's specific components' dimensioning and optimization, here lacking in the prototypal analized device. Therefore, the recorded AC data are not representative of a full-scale, industrial-size device. However, AC data are still fundamental to characterize the functional activity of these devices, allowing to monitor the operation behavior of the whole system and highlighting valuable considerations on the monitored auxiliary behavior.
Numerous experimental tests have been performed, mainly consisting of charge and discharge cycles between ranges of Open-Circuit Voltage (OCV) and state of charge (SOC) set values. The different types of conducted experiments are:

1. Long SOC range tests, with DOD= 80%, to evaluate the battery's real energy capacity and long cycles' efficiency.
2. Reduced SOC range tests, with DOD= 10%, to get efficiency map and check the AORFB's performance consistency.

The first kind of tests aim to track the actual energy capacity of the battery, getting OCV-SOC curves while extracting overall efficiency calculations. From this kind of tests, it was possible to evaluate the battery's C-rate, i.e. the unit measuring the speed at which the battery is fully discharged, with respect to the battery's nominal capacity. Lower C-rates indicate longer discharging time, while unitary C-rate indicate that a full discharge is performed in one hour.
Tests of the second type track the efficiency trends at different power and SOC levels, evaluating the eventual effect of SOC on the battery's performance.

Tests 1: high depth of discharge

High DOD tests have been explored to determine the battery's actual energy capacity. Initially, the OCV trend with respect to SOC has been observed, to monitor the AORFB's electrochemical stability. The following plot illustrates the OCV trend, which has been seen consistent for all the investigated power rates.
The cell V_{dc} trends have then been evaluated with respect to SOC. This voltage value is not the result of a direct measurement, but rather the evaluation of a single cell's average voltage, from the stack's overall voltage measure. As shown in the figure 3.2 , at higher power rates the V_{dc} curves differ from the OCV trend. This is probably due to electrodes' partial polarization and higher contribution of mass transport effect, since higher stack currents affect the velocity of electrochemical reactions [40]. These effects bring higher voltage during the charging phase and lower voltage during discharge.

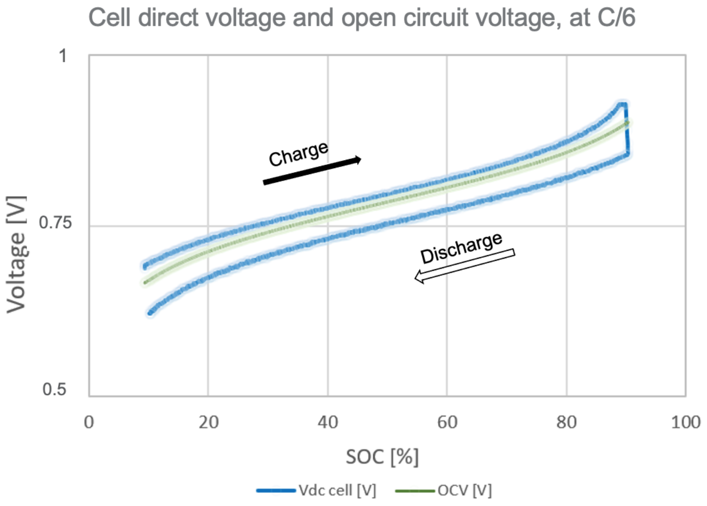

Figure 3.1: Cell's direct voltage (V_{dc}) and Open-Circuit Voltage (OCV) with respect to the state of charge SOC, at low power rate C/6. The trends of V_{dc} and OCV show the system's electrochemical stability.

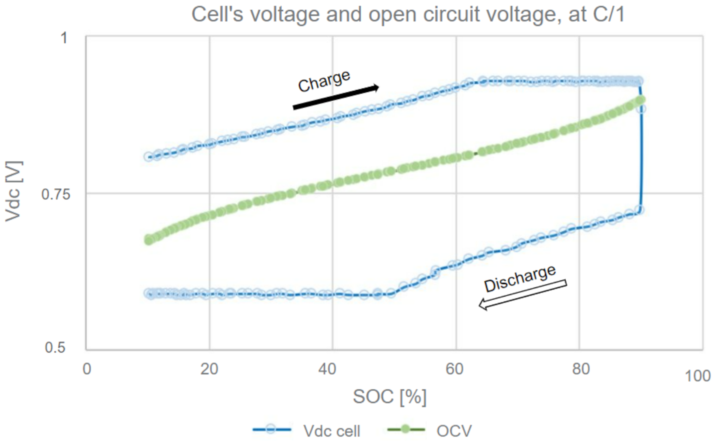

Figure 3.2: Cell's direct voltage (V_{dc}) and Open-Circuit Voltage (OCV) with respect to the state of charge SOC, at higher power rate C/1. As discussed hereafter, the imposed power derating sensitively affects the voltage trend.

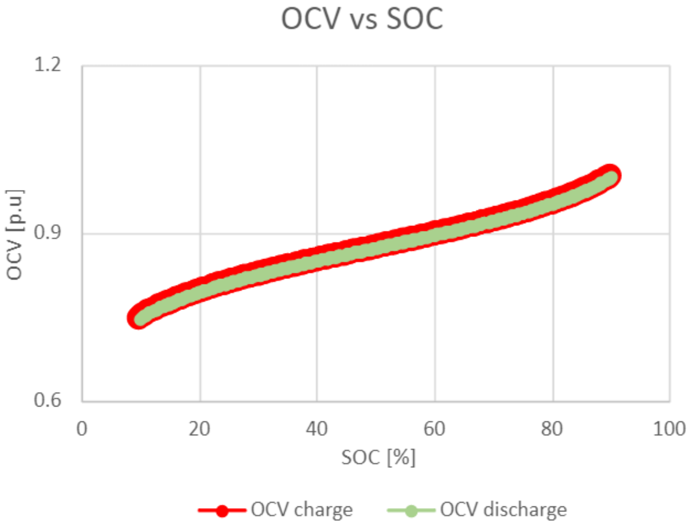

Figure 3.3: Open-Circuit Voltage's trend (OCV) with respect to the state of charge (SOC), measured at low power rate C/6. The consistency of the OCV measures can be appreciated from the accurately overlapping charge and discharge curves.

Charge and discharge cycles have been carried out at different power levels. In this work, the C-rate is defined as the power value required to discharge at constant rate a battery of "C" capacity in a given target time. The C-rate is reported in the form C/X, where X is the target discharge duration, in hours; thus, C/3 is the constant power rate needed to fully discharge the available capacity of the battery in 3 hours. Due to the specific control variable available for the analysed storage system, the C-rate here is referred to a DC power setpoint. Both V_{dc} and I_{dc} have been recorded at different C/Xs, to evaluate the system's operational performance. As shown in the figures 3.5 and 3.4, while for higher C/Xs the current has a very stable linear trend and a consequent symmetrical SOC behavior, in case of high power operations the plot shows a high curvature of the current due to derating. This leads to an additional time required to complete both recharging and discharging phases. This also shows how long-duration applications can constitute AORFBs' design application, while higher power operation requires significant derating to preserve the system's proper functioning while safeguarding the battery's lifetime. Further experimental investigation had been undertaken, to better examine derating's actual impact at many C/Xs, and to have a comprehensive "map" of the AORFB's operational area. This derating, at first deducted from experimental observations, has been confirmed by the battery system's providers, who confirmed the actual reduction of power at higher power rates. This safety measure, operated by the PCS, is considered necessary in order to preserve the batteries' safety conditions, preventing stack materials' damage, i.e. additional stresses on the electrodes and membrane separators. The actual "State of available power" (SOAP) is shown in the figure 3.6.

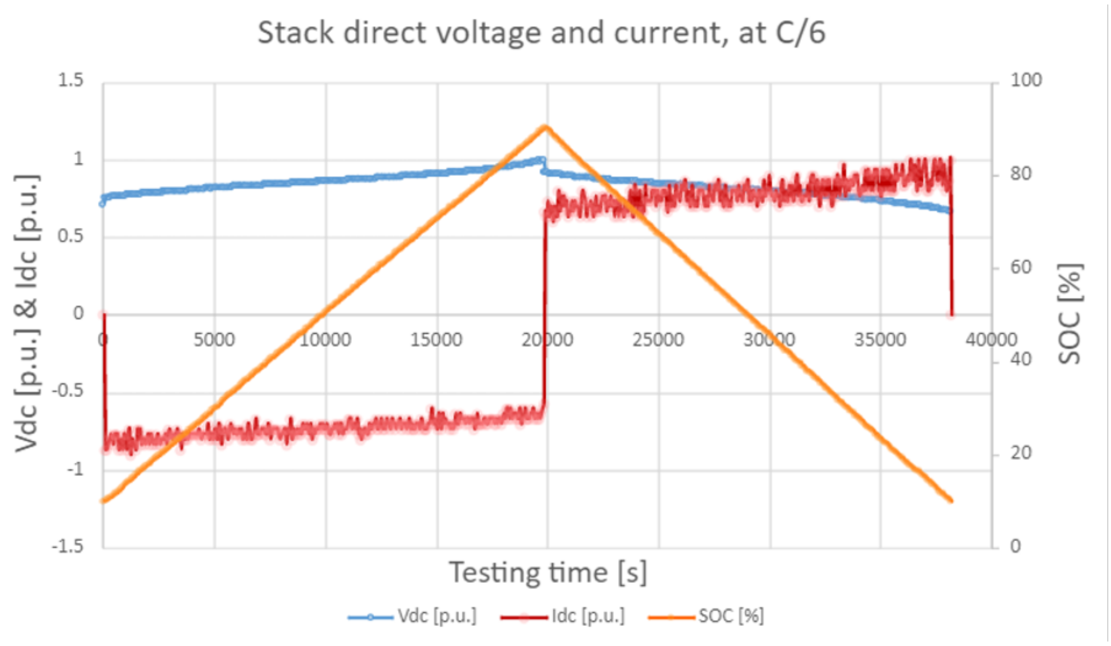

Figure 3.4: Normalized trends of stack's direct current (I_{dc}), direct voltage (V_{dc}), and state of charge (SOC) at low power rate C/6. The currents trend is actually linear in both charge and discharge, with only few ampere of difference from the nominal value, even if here this difference may seem more impactful.

To have a factual grasp of this operating setting, the derating has been examined by

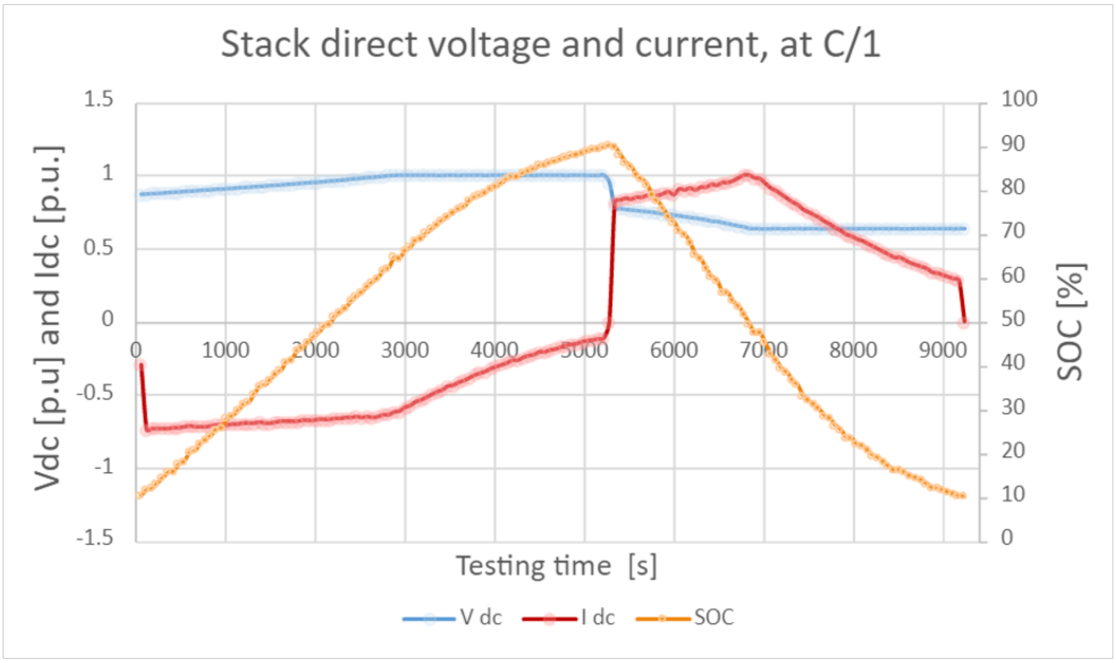

Figure 3.5: Normalized trends of stack's direct current (I_{dc}), direct voltage (V_{dc}), and state of charge (SOC) at high power rate C/1. Here the power derating imposed by the PCS is visually evident, showing the system's behavior when operating at specific values of SOC.

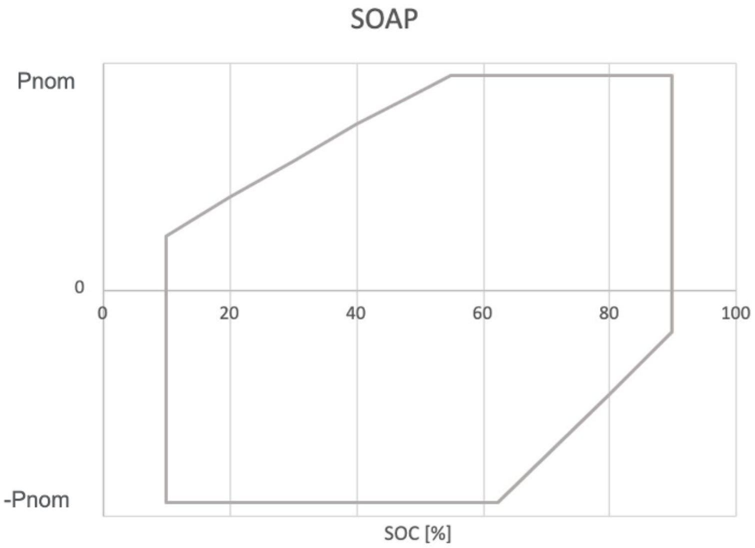

Figure 3.6: State of available power (SOAP) imposed by the PCS, with generators' sign representation (negative for charge, positive for dicharge). The SOAP provides a visual map of the derating imposed on the battery's operative behavior.

observing how fast the BMS activates it. A specific dedicated test has been undergone, to verify if the derating behavior, activated by the BMS, works only during complete cycles, or instead if it is applied for any generic operational condition. From SOC =10%, the battery has been charged until SOC =60% and immediately turned off. Immediately after, discharge coniditions have been performed, to see the responsiveness of the battery and how quickly the derating is effectuated.
As shown in figure 3.7, PCS's derating is quite responsive, proceeding to reduce the current amount almost immediately after the battery is activated again.
Including all experimental results, the operational curves for high DOD have been plotted together with the "theoretical" SOAP indicated by the providers. The figure 3.8 shows the curves for the evaluated power rates, and the battery's behavior for long tests. As displayed in the plot, the operational conditions showed a behavior slightly better than the expected nominal SOAP. While keeping the AORFB's operation within the SOC limits, it is evident here how real cycles behave, and how energy and efficiency calculations will be impacted by the derating. Together with the V_{dc}, I_{dc} and P_{dc} evaluation, the battery capacity is calculated, evaluated as both discharge capacity [Ah] and nominal energy capacity [Wh]. The figure 3.10 shows how the DC discharge capacity is constant for long-duration applications, while for relatively higher power conditions the capacity decreases significantly. These systems, although exploiting their full potential for higher energy conditions, are flexible for the required application, where the energy capacity is kept at relatively high levels even at higher power.

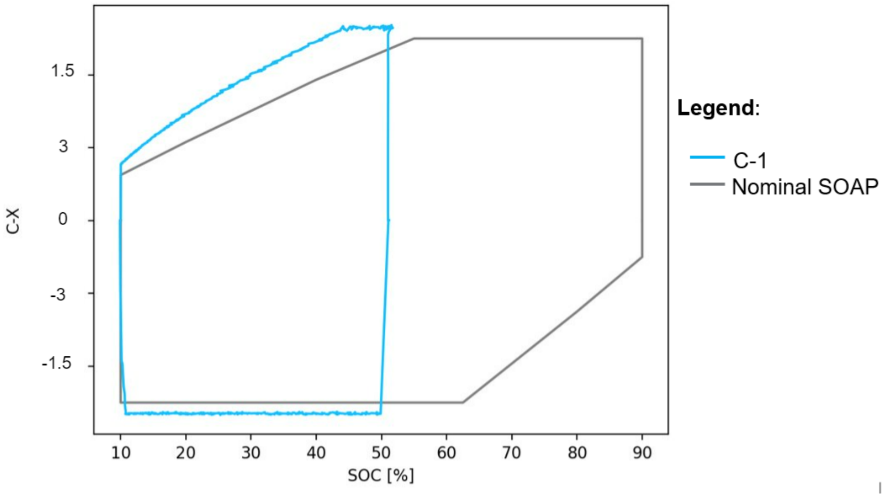

Figure 3.7: Derating verification curve. After being partially charged until 50% of SOC, the battery has been disconnected and immediately discharged. This test has showed that the derating is immediately activated as soon as the system is operative again, proving the actual operating power range and behavior.

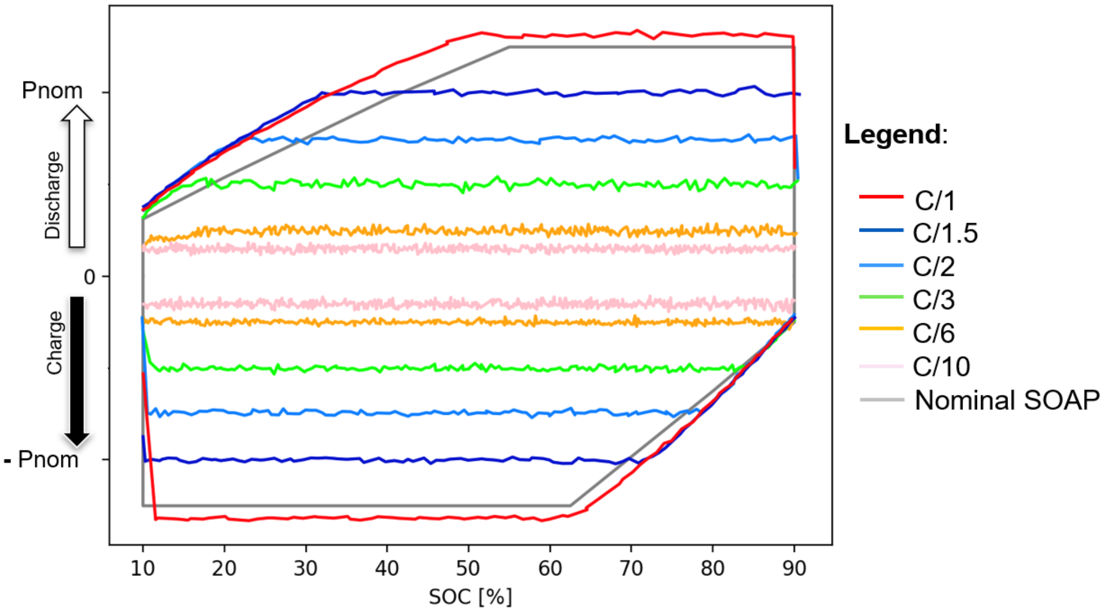

Figure 3.8: State of available power (SOAP) curves for all the different evaluated C/rates over the full-DOD tests. The experimental campaign has verified the actual power operating area, which is slightly higher than the theoretical performance indicated by the technology's providers.

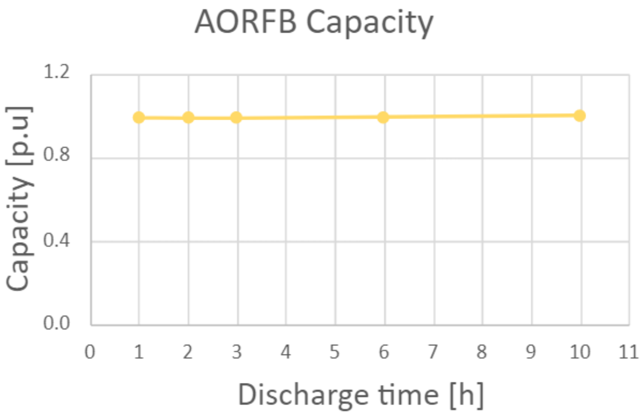

Figure 3.9: Battery's trend of the average recorded values of discharge ampere-hour [Ah] capacity, measured during the discharge phase. The cponsistent linear trend throughout the measured timeframes represents a further evidence of the electrochemical stability performance of the AORFB.

From the gathered data, DC efficiencies have been obtained and quantified, for

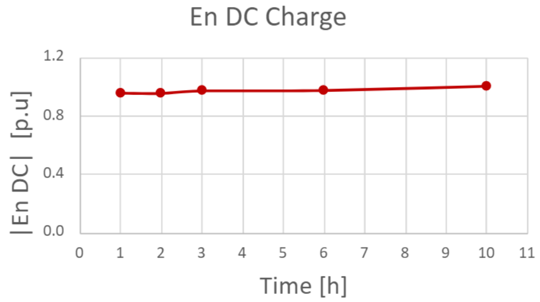

Figure 3.10: Average values' trend of direct current (DC) Energy, experimentally measured during the charging phase. The results show a very linear and stable trend for all the investigated nominal charging time durations.

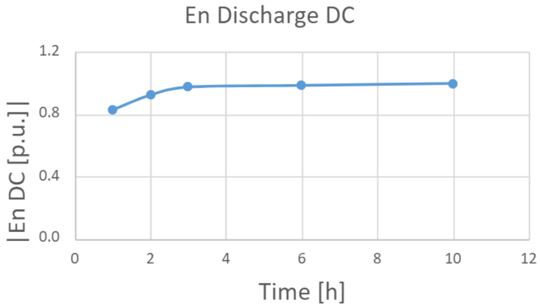

Figure 3.11: Average values' trend of direct current (DC) Energy, experimentally recorded in the discharging phase. The results show a linear trend for time durations above 2 hours, with a decrease in value for lower discharge intervals.

different power rates. Introducing the formulae for efficiencies [41]:

$$\eta_{\mathrm{DC}} = \frac{\int_0^{t_d} P_{\mathrm{discharge}} dt}{\int_0^{t_c} P_{\mathrm{charge}} dt} \tag{3.1}$$

$$\eta_{\mathrm{AC}} = \frac{\int_0^{t_d} P_{\mathrm{discharge}} - |P_{\mathrm{AUX,disch}}| dt}{\int_0^{t_c} P_{\mathrm{charge}} - |P_{\mathrm{AUX,ch}}| dt} \tag{3.2}$$

The values for energy efficiency are definitely steady for higher energy applications, at over 80%, while for the highest power rate the efficiency is above 70%. The obtained values are overall competitive with VRFB commercial current systems [32].

It's possible to deduce that for higher power rates, a lower efficiency has been recorded. The most plausible explanation for this correlation involves the increase of mass transport phenomena of the active organic molecules.

As introduced in the figure 1.5 in Chapter 1, electrochemical cells' voltage is reduced

at high currents due to mass transport phenomena. In fact, the diffusion of active molecules across the separator membrane are enhanced at higher current rates. This becomes even more relevant in AORFBs, where organic molecules within the cells are prone to crossover phenomena, which constitute one of the main issues affecting organic RFBs' performances [29]. Therefore, the increase of diffusion phenomena lead to a consequent increase of the diffusion overvoltage losses, which presents detrimental effects on the battery's efficiency.
However, the efficiency decrease observed for high current application should examine this theoretical concentration issues in the electrolytes with dedicated and specific measurement equipment, which eludes from the purpose of this work.
Still, for lower power rates, the efficiency trend is remarkably stable, proving AORFB most suited operational performance for long-duration applications.

C/X	η DC [%]
1	72
2	83
3	85
6	86
10	86

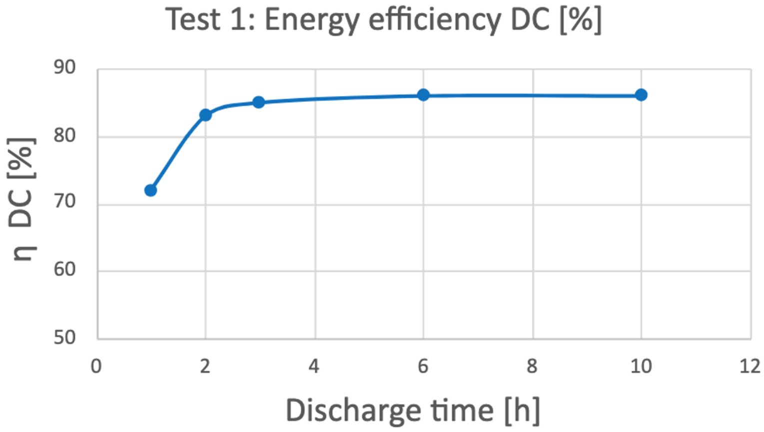

Figure 3.12: Average experimentally measured values of direct current (DC) efficiency. The trend shows consistent values above 85% for discharge duration times higher than 2 hours, while below this threshold the efficiency is significantly reduced to circa 72%. This reduction is most probably due to lower electrodes' kinetics, occurring at higher power rates.

As introduced at the beginning of this chapter, AC values data have been analyzed as well, but due to the prototypal structure of the studied system, AC results are not representative of full-scale, real-size industrial devices. Regardless, the evaluated AC results are still fundamental to characterize the functional activity of these devices, and the most relevant considerations are here presented. The auxiliary power consumption includes pumps, BMS and PCS activation throughout the whole battery's operability.

$$P_{\text{AUX}} = P_{\text{pumps}} + P_{\text{BMS}} + P_{\text{PCS}} \tag{3.3}$$

The "DC" values quantify and evaluate the AORB's electrochemical characteristics and performances, while "AC" values consider the global performance of whole

system, accounting each and every necessary component for the battery's complete functioning. The auxiliary power consumption includes pumps, BMS and PCS activation throughout the whole battery's operation. The AC roundtrip efficiency values have been experimentally evaluated as well. However, due to the lack of optimization for the prototype studied system, the power consumption due to auxiliary (AUX) elements affect the studied AORFB prototype's performance more deeply than they would in an industrial-scale system. In particular, pumping devices have the heaviest impact on the auxiliary power, continuously operating to ensure the electrolytes flow into and from the stack.
The optimization of flow rates and consequent pumps' design require a specific sizing that could not have been realized on the prototype studied in this work. Moreover, the power consumption from PMS, PCS and BMS (for example, from the inverter's operation) also require ad-hoc optimizing constructive implementations. The AC performance is impacted by all the above-mentioned concurrent factors, making the obtained results not completely representative for real-sized devices.

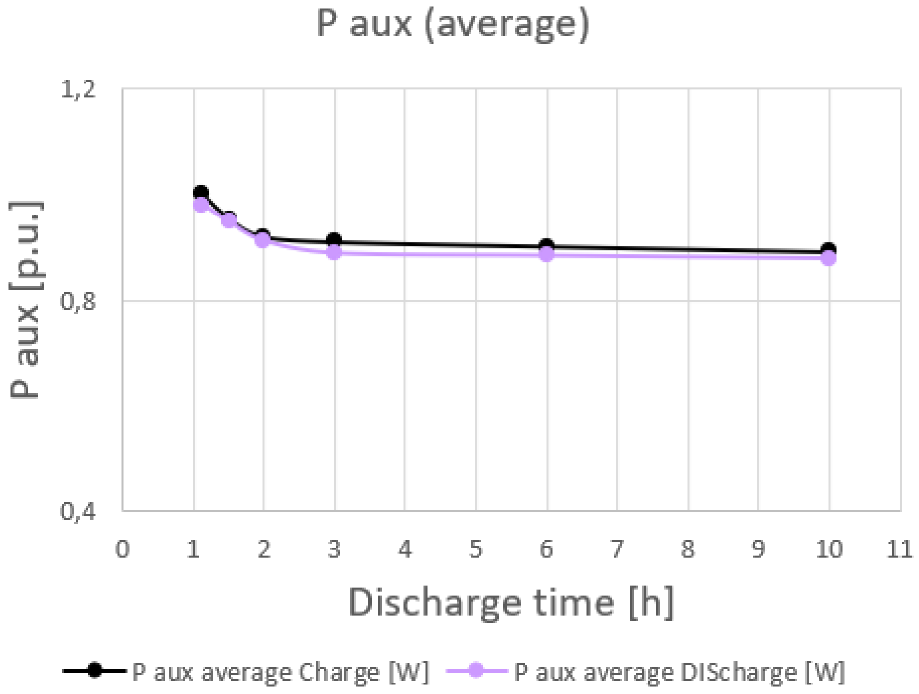

Figure 3.13: Average standard auxiliary consumption (AUX) trend, for both charge and discharge phases. The recorded results indicate how the auxiliary consumptions, with the highest contribution of pumping, is not linearly dependent on the battery's power rate. The high impact of AUX would be reduced with design optimization in s real-case device.

The experimental campaign has showed that a crucial factor for optimal design might involve the deployment of modular pumps, which have the potential to drastically reduce the pumping auxiliary consumption by making it proportional to the battery operating power, thus constituting a real game-changer for RFB's industrial development.

Not-optimized system's average auxiliaries trends for both charge and discharge, including pumps, inverter and BMS' consumption, are shown in 3.13. Experimental points are represented in adimensional units, normalized with respect to the nominal auxiliaries power. Even with slightly higher value at high power rates (lower discharghe time), auxiliaries consumption proves to be almost constant in both charge and discharge, independently of the power rate (with a maximum variation of -13% with respect to nominal AUX consumption).

The auxiliary power, measured with a negative sign since it is absorbed by the AORFB, is plotted in its absolute value in figure 3.13. The average recorded auxiliary consumption does not vary significantly with the requested power rate. Although the needed power to be provided by the stack depends on the amount of electrolyte needed to produce it, in here the pumps' consumption are significant even at lower power rates.

Interesting considerations can be highlighted about the need for heating. Unlike more traditional electrochemical batteries, this aqueous RFB do not require air-conditioning systems to decrease the temperature rising due to current's Joule losses in the stack. However, to keep the electrolytes' nominal values of energy density, viscosity, and other fluid-dynamic parameters, the PCS keeps the electrolytes' temperatures above a certain threshold value, which is circa 21 °C. If the recorded temperature is lower, a local heating auxiliary device heats up the electrolytes until the temperature goes above the set point.

As shown in figure 3.14, the heating device's activation increases the auxiliary power consumption up to almost twice as much as ordinary auxiliaries. Although this factor surely has to be kept under control throughout operational conditions, the experimental experience recorded only few cases with the occurrence of heating activation, and all those cases included more than three days of the system's total inactivity, with the system disconnected from the mains.

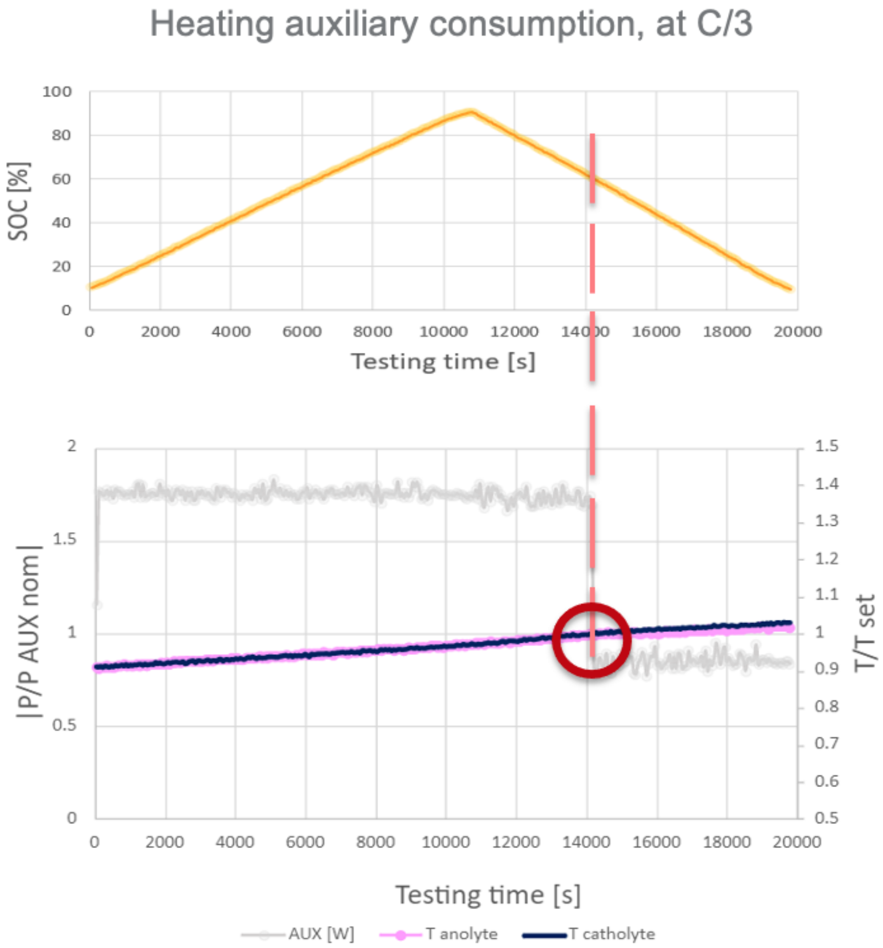

Figure 3.14: Auxiliary consumption (AUX), including heating devices activation for electrolytes' temperature below 21°C, and consequent significant auxiliary increase. As soon as the set temperature is reached, AUX value instantaneously returns to nominal values.

Tests 2: Reduced SOC range tests

The AORFB's behavior for reduced intervals of SOC has been performed through an experimental test campaign, with procedural steps analogue to the tests conducted by Politecnico di Milano in [42].

Traditionally, electrochemical devices' efficiencies are referred to nominal conditions, which are usually quite different from the actual operational ones. Moreover, traditional battery technologies are sensitive to the applications' SOC range, and this effect becomes more relevant for relatively shorter cycles.

Experimental tests at low SOC intervals have been performed, within three SOC ranges of 10%, examining the same power rates applied during the higher DOD tests, but this time focused on three different SOC ranges. The DC and AC efficiencies for reduced SOC ranges have been measured, in order to check whether and how much the SOC level influences the battery operation during these "faster" cycles. Also, the second type of tests' results have been compared to high DOD tests, to check the device's performance consistency at different conditions. The explored cases are:

1. SOC range: 20-30%
2. SOC range: 50-60%
3. SOC range: 80-90%

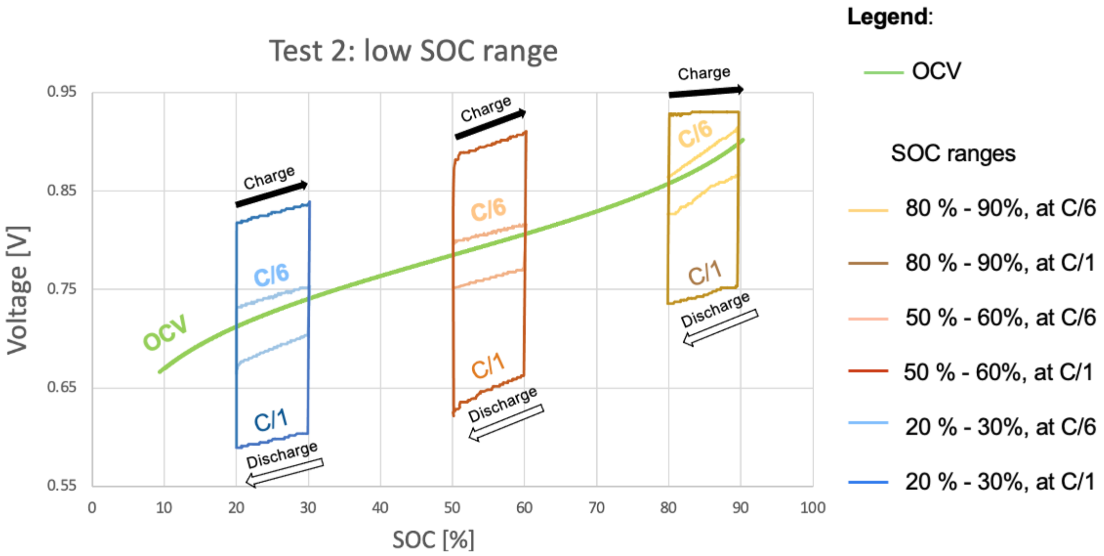

Figure 3.15: Reduced SOC interval tests at reduced state of charge (SOC). These tests evaluate the possible influence of SOC intervals on the device's performances.

The reduced SOC interval tests' experimental results are displayed in figure 3.16. For every SOC interval, numerous tests at given power rates have been performed, and the average energy efficiency result for each power rate has been indicated. The recorded average efficiency results show very similar values for almost every SOC range. The vast majority of the other, for all SOC ranges and at any power rate, present discrepancies lower than 0.5%.
The highest discrepancy of efficiency value has been recorded for the highest power rate at SOC range (80%-90%), showing a discrepancy of circa 2.5% with respects to the other SOC intervals at the same power rate.
The factor that most probably affects this large discrepancy is attributed to the derating effect, affecting the charging phase at high SOC levels and bringing higher efficiency values.
However, this last assumption should be verified with further specific tests at the level of individual cells, involving dedicated measurement equipment, which eludes from the purpose and methodology of this work.

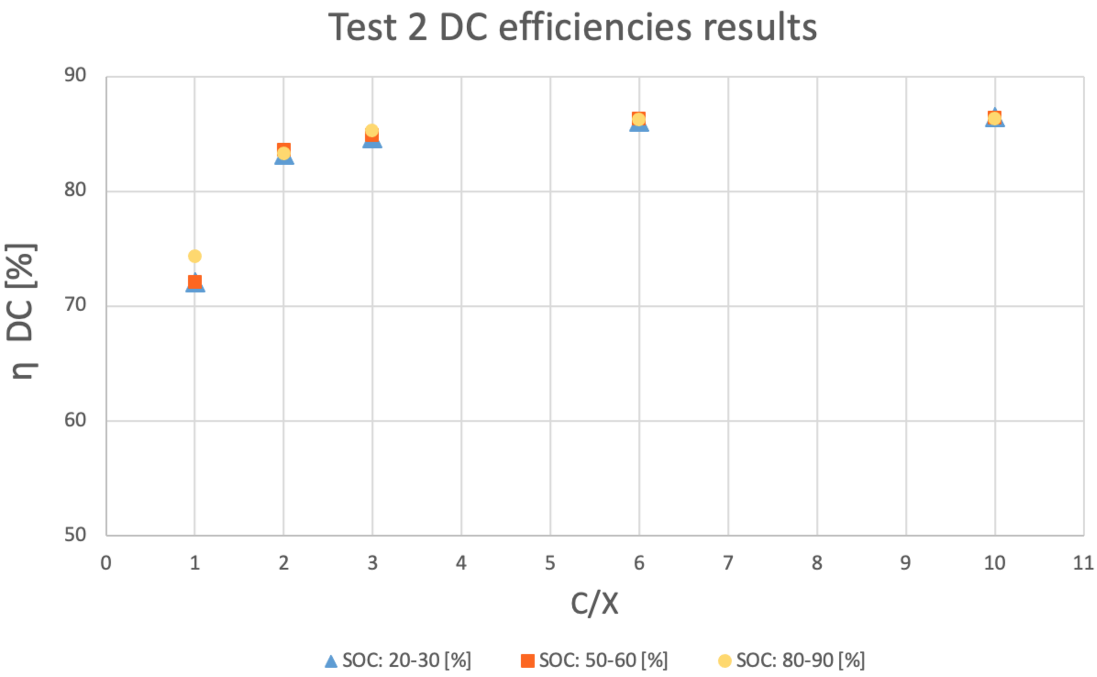

Figure 3.16: Direct current (DC) average efficiencies values for different reduced state of charge (SOC) ranges. The experimental campaign showed how the efficiency results are quite consistent even at different SOC intervals.

As anticipated, the reduced SOC intervals' results have been compared to the efficiency values of high DOD experiments. The values showed in table 3.1 indicate how the shorter cycles bring very similar DC efficiency results with respect to the

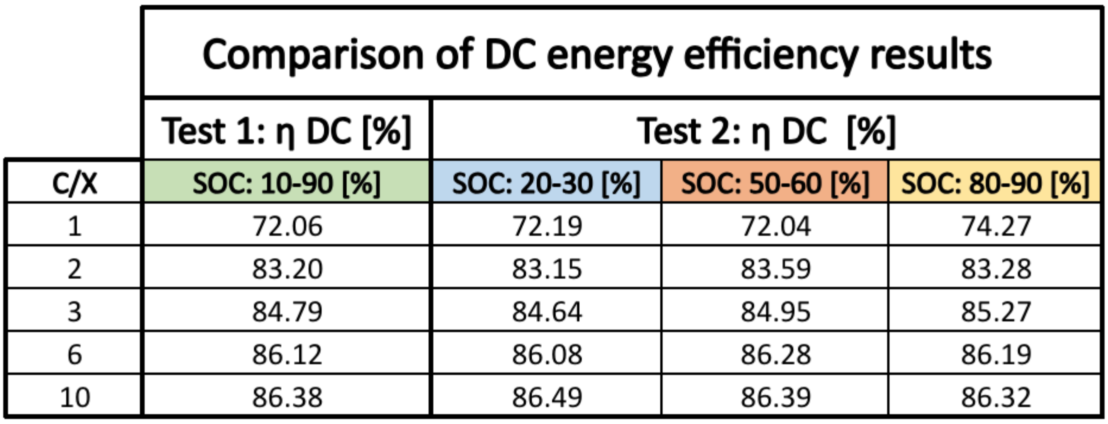

	Comparison of DC energy efficiency results			
	Test 1: η DC [%]	Test 2: η DC [%]		
C/X	SOC: 10-90 [%]	SOC: 20-30 [%]	SOC: 50-60 [%]	SOC: 80-90 [%]
1	72.06	72.19	72.04	74.27
2	83.20	83.15	83.59	83.28
3	84.79	84.64	84.95	85.27
6	86.12	86.08	86.28	86.19
10	86.38	86.49	86.39	86.32

Table 3.1: Direct current (DC) average Efficiencies values for different reduced state of charge (SOC) ranges: The experimental values prove how the main influence on the AORFB's performance lies in the application's power level.

longer duration tests.
This experimental results' consistency highlights how, in the AORFB device, the DC efficiency performance is significantly affected by the application's power rate, while the operational SOC level has a significantly lower influence.
The DC efficiency results recorded for AORFB show an important different feature with respect to most traditional battery technologies.
In particular, as indicated in [42], Lithium batteries' behavior is influenced by the SOC level of the required energy application. Charge and discharge operations, in fact, are performed through the intercalation of Lithium ions within the anode and cathode materials (generally through the insertion mechanism of Lithium ion in the lattice). However, the Lithium ions' intercalation induces electrodes' crystal lattice's deformation, which shows high sensitivity to the state of charge. This deformation can increase the battery's internal resistance, and high SOC might hinder the battery's overall capacity of effectively storing energy, thus affecting the battery's efficiency performance.
On the other hand, due to their intrinsic constitutive elements, AORFB liquid molecules perform redox chemical reactions in correspondence of the active area of the porous carbon felt. However, during and after the redox reactions, liquid organic molecules do not modify the crystal lattice structure of the felts' reactions sites, and organic molecules' reactions do not induce deformation in the felts. Therefore, the SOC influence on the internal resistance is reduced, and the AORFB results have proved that SOC does not significantly impact the DC efficiency performance of the AORFB device.

Consideration on AC values for Test 2

During the experimental campaign, the AC values for low SOC range cycles have been evaluated as well for the SOC ranges of 20-30%, 50-60%, and 80-90%.
The main sensitive differences among the "faster" cycles have been witnessed for the 50-60% range: at C/3, the recorded efficiency increased up to 3% with respect to the other SOC ranges, while the other results witnessed an increase of circa 1%. This efficiency result difference is mostly due to the reduced influence of derating, allowing to bring the full power of the AORFB in a reduced period, thus reducing the auxiliary consumption's effect.
Moreover, the AC results of reduced SOC intervals tests recorded very similar values with respect to the AC results of high DOD tests (with higher values' aligning with the SOC range of 50-60% SOC range).
The results have provided further practical evidence that not only the DC performance, but also the full system's efficiency records no significant dependence on SOC, but rather from the operative power levels.
Finally, in all three SOC ranges, the auxiliary consumption has been examined at different C-rates. From the measurements' results, no relevant difference in auxiliary values has been measured, confirming the average steady consumption values recorded for full SOC range cycles, constituting a constant "base load" throughout the entire device's operation.

3.1.2 Final experimental considerations

The experimental experience has proven the effective operational behavior of the examined AORFB device.

From an operational point of view, the AORFB system showed robustness and ease of control, with high responsiveness for both charging and discharging phases. After the installation by the technology providers, no electrolytes' leakages have been detected, showing the optimal tightness of the system's junctions and gaskets, not to be taken for granted in a prototype device. With respect to VRFB, the tested AORFB technology requires lighter thermal management, as it can operate at high environmental temperatures with no need for cooling. A dedicated heating system is embedded only to ensure full-performance operations when electrolytes temperatures go below 21°C.

In both long and short cycles, the system showed high operational consistency in efficiency and energy performance. Different SOC ranges don't significantly affect the results, which have proven the best values for duration applications longer than three hours. The recorded values for DC efficiencies range from around 86% at longer durations, to circa 72% for higher-power operations. The outstanding DC results are highly competitive with the present, more mature VRFB technology (indicated in the reference PNNL 2022 report [32]). Exploring AC results, the auxiliary power consumption constitutes the major opportunity for a future improvement. Expected AC performance is currently under implementation. Nevertheless, applying due optimized design and auxiliary management, AORFB systems' electrochemical performance foresees AC efficiencies aligned with VRFB present values. In five years from now, with optimized pumping devices and converters' sizes, the forecast roundtrip efficiency for the tested AORFB technology will reach values between 60% and 67%.

Moreover, the long-duration potential can be perfectly matched with the core feature of AORFBs' modularity, allowing a relatively easy potential scaling-up of these systems to increase the operational discharge duration to over 10 hours, by only increasing the electrolyte's quantity and the tanks' number and/or size. Containerized units (with cell stacks, balance-of-plant devices and power conversion systems) of hundreds of kW can become the unit storage module to be coupled with external tanks, in order to easily scale up to meet MW/MWh requirements of large scale systems.

Ultimately, the experimental campaign showed how AORFB technology is not only a very promising energy storage alternative to current solutions, but it has been proved to be perfectly suitable for long-duration applications, for both stability and efficiency performances, especially for operations longer than 3 hours, with forecast ease of scaling-up and operation flexibility depending on the desired energy. It must be noted that research on AORFB technologies is still ongoing to select more and more performing molecules, optimise auxiliaries management and system overall efficiency and improve electrolytes stability over the current target of 20 years.

3.2 Techno-economic results

3.2.1 AORFB results

The techno-economic calculation results are displayed hereafter. Using the set of equations and the methodological steps described in Chapter 2, the Python code has been implemented, providing Capex, Opex and LCOS as techno-economic outputs, displayed in figure 3.2.

As described in the introductive chapter, due to their intrinsic organic characteristics, AORFB batteries witness an energy performance's annual degradation,which has been set equal to 1%. This value has been indicated by the technology provider, as well as from literature references for real-case AORFB systems [38].

For current commercially available solutions, as well as the tested device of this work, AORFB present RTE values around 50%. Nonetheless, efficiency values for AORFB is foreseen to reach 65% within the upcoming 5 years.

Economic results for Capex, Opex and LCOS values are displayed in the table 3.2, for different roundtrip efficiencies values of 45%, 55% and 65%. The sensitivity on RTE, while Capex and Opex are clearly constant, is shown in the results of LCOS, for different battery's power sizes and discharge durations.

Also, the values for the AORFB system device, experimentally analyzed in chapter 2, are reported in the table 3.17. These results illustrate the costs for the specific power size and energy capacity of the battery device examined in this work, including the derating verified in the experimental part.

On the other hand, the results obtained in 3.2 are all evaluated without the derating application. This because derating is an operative condition decided by the technology providers, and can be programmed and modified to suit the needed application.

More detailed considerations about the eventual derating applications are illustrated in the next section and in figure 3.19.

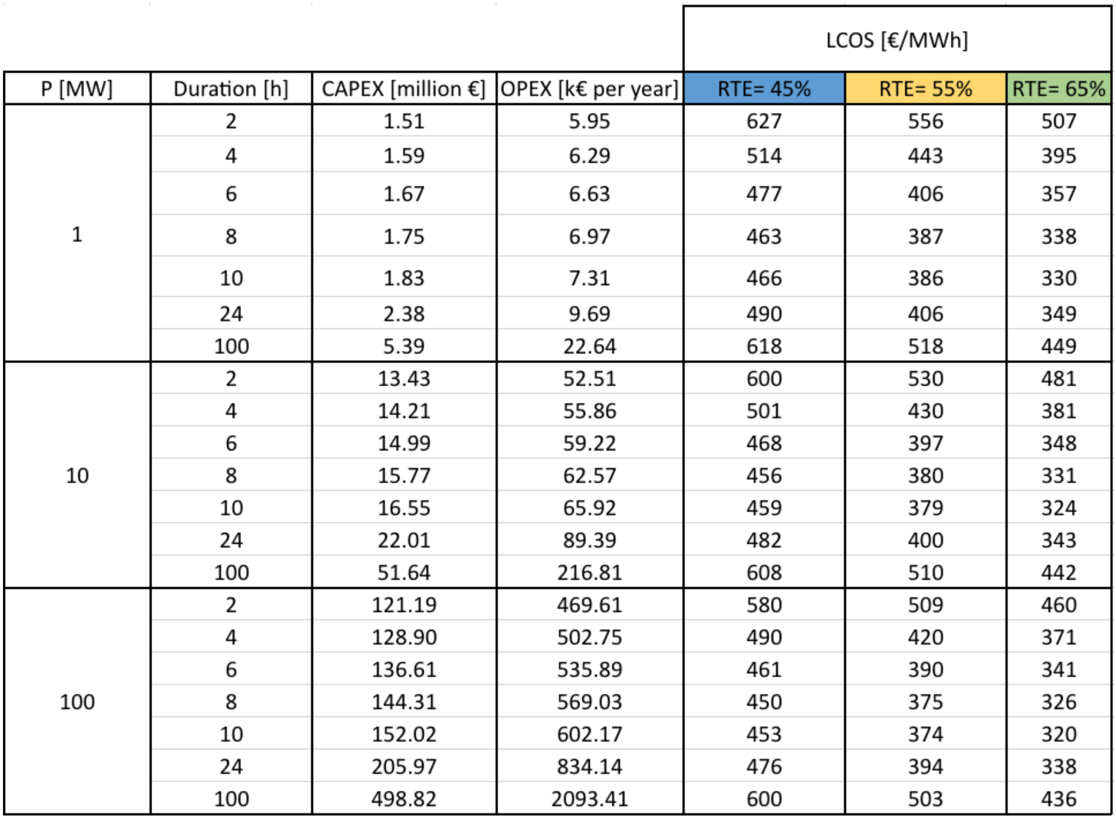

				LCOS [€/MWh]		
P [MW]	Duration [h]	CAPEX [million €]	OPEX [k€ per year]	RTE= 45%	RTE= 55%	RTE= 65%
1	2	1.51	5.95	627	556	507
	4	1.59	6.29	514	443	395
	6	1.67	6.63	477	406	357
	8	1.75	6.97	463	387	338
	10	1.83	7.31	466	386	330
	24	2.38	9.69	490	406	349
	100	5.39	22.64	618	518	449
10	2	13.43	52.51	600	530	481
	4	14.21	55.86	501	430	381
	6	14.99	59.22	468	397	348
	8	15.77	62.57	456	380	331
	10	16.55	65.92	459	379	324
	24	22.01	89.39	482	400	343
	100	51.64	216.81	608	510	442
100	2	121.19	469.61	580	509	460
	4	128.90	502.75	490	420	371
	6	136.61	535.89	461	390	341
	8	144.31	569.03	450	375	326
	10	152.02	602.17	453	374	320
	24	205.97	834.14	476	394	338
	100	498.82	2093.41	600	503	436

Table 3.2: Techno-economic results for different power sizes and roundtrip efficiencies scenarios. While CAPEX and OPEX values are the same, the increase of RTE significantly reduces the LCOS values.

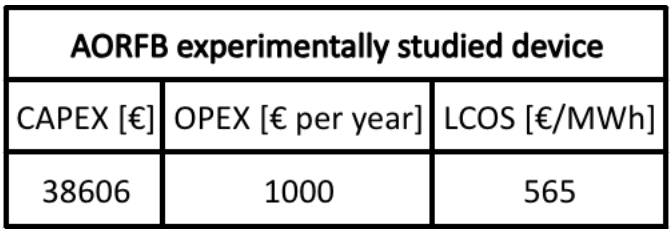

AORFB experimentally studied device		
CAPEX [€]	OPEX [€ per year]	LCOS [€/MWh]
38606	1000	565

Figure 3.17: Economic results for the studied device's size and discharge duration. Although it is a prototypal experimental system, the battery device studied in this model has been considered as a full AORFB system, evaluating all the techno-economic features considered in this model.

3.2.2 Comparison between AORFB and VRFB results

Comparison between redox-flow technology, to see the readiness level of AORFB with respect to more mature vanadium-based already commercialized devices. Calculations for different power size were performed, comparing the obtained results with VRFB values [43]. The results are displayed in the figure 3.18. As expected, both Capex and Opex are lower in AORFB, due to lower ELY cost. For current battery system devices, either prototypes or fully-developed ones, AORFB present average RTE values around 50%, while VRFB offer values of 65%. As shown in the plots below, this results in a higher LCOS for organic batteries. Nonetheless, efficiency values for AORFB is foreseen to reach 65% within the upcoming 5 years. With such improvement in RTE value, AORFB will have a LCOS low enough to become competitive with current VRFB technologies, while still presenting cheaper and easily procurable raw materials, and less safety and environmental issues. For discharge time lower than 10 hours, the contribution of E_b prevails, causing a reduction of LCOS. However, for higher durations the CAPEX contribution becomes more dominant, thus increasing the LCOS value. A specification is here overdue: the evaluated values showed here are referred to LCOS results evaluated without the derating evaluated and verified in the previous chapter. However, in the examined AORFB system, the operating conditions and consequent LCOS values are highly influenced by the derating, which reduces the the total energy production up to 71% for C/1 power rates application. Relative values with applied derating, for different discharge duration conditions, are here compared to VRFB values and AORFB without derating.

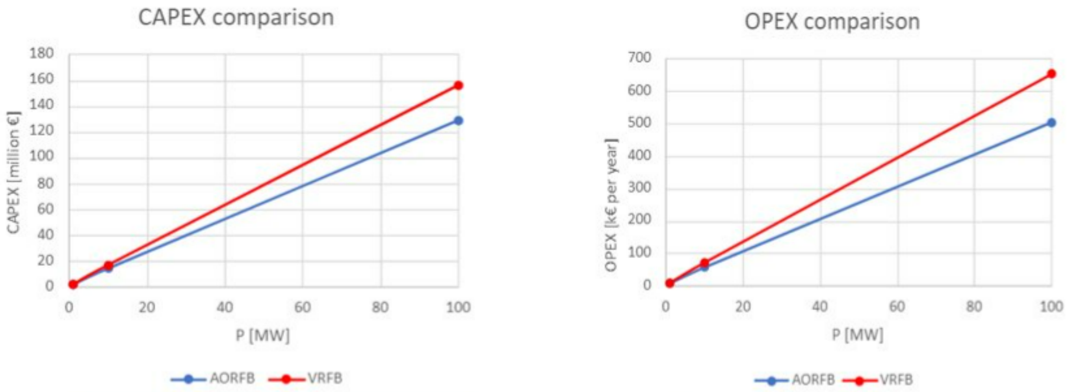

P,n [MW]	CAPEX AORFB [million €]	CAPEX VRFB [million €]
1	1.59	1.84
10	14.21	16.84
100	128.90	156.01

P,n [MW]	OPEX AORFB [k€ per year]	OPEX VRFB [k€ per year]
1	6.29	7.72
10	55.86	70.57
100	502.75	651.81

Figure 3.18: CAPEX and OPEX comparison between AORFB and VRFB, considering the power size variation. As expected, the expenditures of the organic technology records lower values with respect to vanadium-based devices, due to the drastic reduction of electrolyte cost.

As displayed by the results, the derating significantly reduces the LCOS final value. For higher power rates' applications, the AORFB's value with applied derating indicate how AORFB become more expensive than VRFB for a time duration

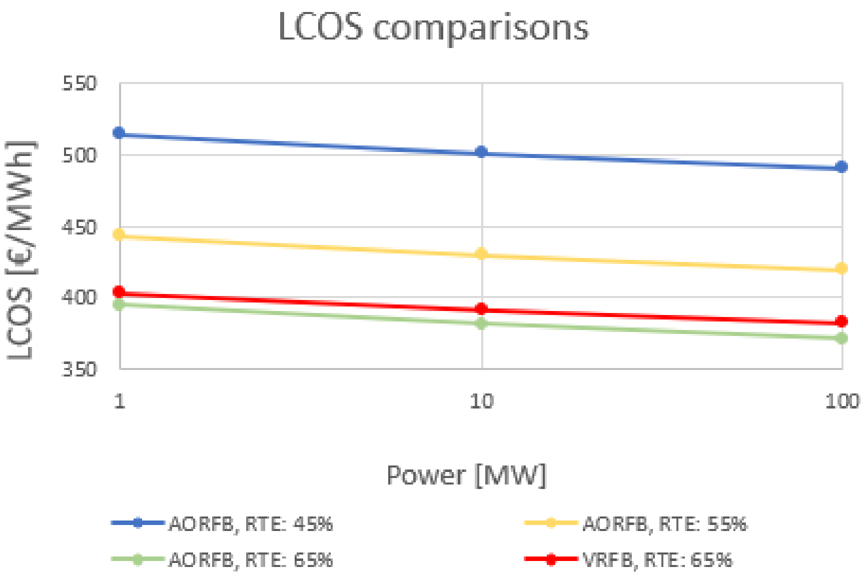

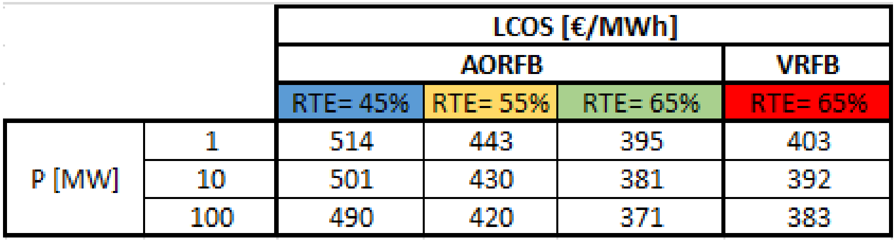

		LCOS [€/MWh]			
		AORFB			VRFB
		RTE= 45%	RTE= 55%	RTE= 65%	RTE= 65%
P [MW]	1	514	443	395	403
	10	501	430	381	392
	100	490	420	371	383

Figure 3.19: LCOS comparisons between AORFB and VRFB, at different roundtrip efficiency (RTE) values. Even accounting organic degradation, in order for AORFB to be competitive with VRFB, a minimum value of RTE=65% has to be provided.

lower than 4 hours.

However, the power derating application has been decided by the technology provider to better preserve the studied AORFB device's operative lifetime, but literature references do not indicate the mandatory application of such precautionary measure, the following techno-economic results do not include the above mentioned power derating.

Final considerations have been undertaken for the discharge duration during operating applications. As explained in the previous section, before 10 hours the Energy effect reduces LCOS values, while for more than 10 hours the CAPEX contribution increases the LCOS.

These plots also show how the discharge timeframe between 8 and 10 hours is the most economically convenient. Moreover, the value for 24 hours is still way lower than for timespans below eight hours, as further validation of AORFB systems optimal performance for long-duration storage applications.

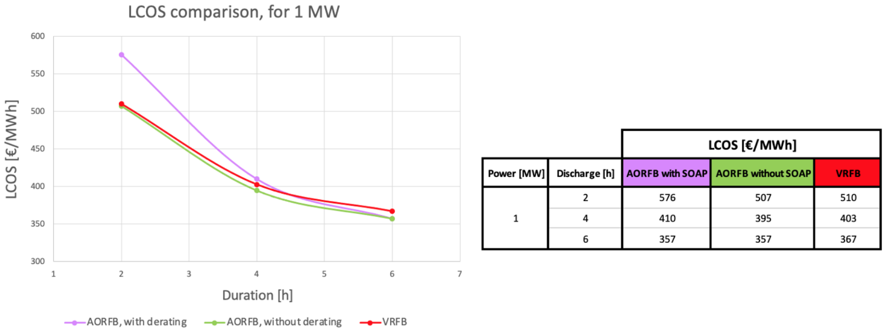

		LCOS [€/MWh]		
Power [MW]	Discharge [h]	AORFB with SOAP	AORFB without SOAP	VRFB
1	2	576	507	510
	4	410	395	403
	6	357	357	367

(a) LCOS comparison, 1 MW

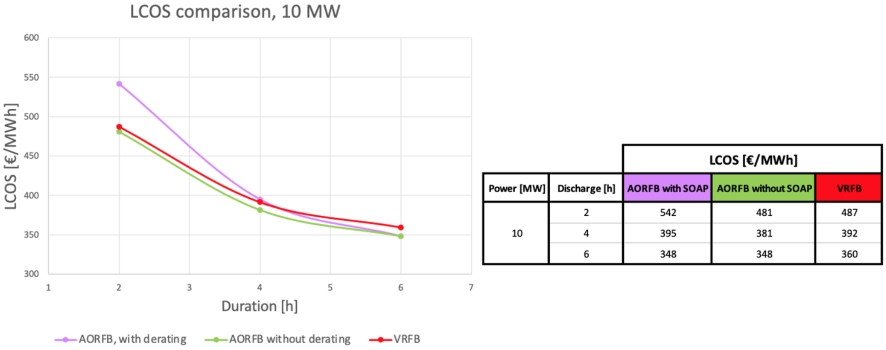

		LCOS [€/MWh]		
Power [MW]	Discharge [h]	AORFB with SOAP	AORFB without SOAP	VRFB
10	2	542	481	487
	4	395	381	392
	6	348	348	360

(b) LCOS comparison, 10 MW

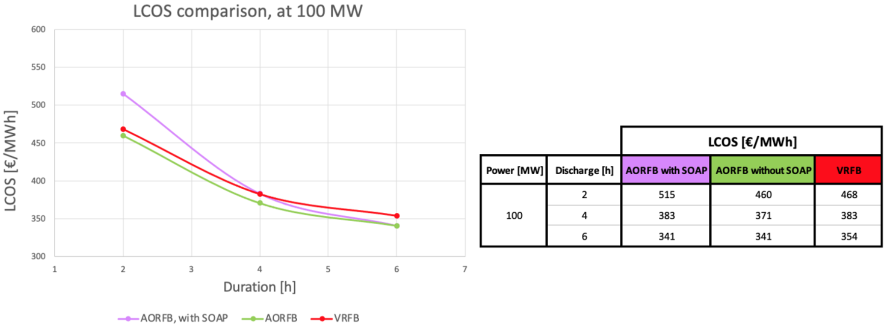

		LCOS [€/MWh]		
Power [MW]	Discharge [h]	AORFB with SOAP	AORFB without SOAP	VRFB
100	2	515	460	468
	4	383	371	383
	6	341	341	354

(c) LCOS comparison, 100 MW

Figure 3.20: LCOS comparison between VRFB and AORFB, with a sensitivity analysis on the eventual derating application. For nominal power sizes of 1, 10 and 10 MW, the applied derating reduces the produced energy up to 70% of nominal energy, with higher reductions for short-time applications. Accounting the derating for AORFBs, the LCOS value increases significantly, making organic technology less competitive than VRFB. However, derating procedures are decided by the technology providers to preserve the battery stability. Therefore, derating consists of a precautionary measure that, with increasing technological know-how, is destined to be removed in the near future.

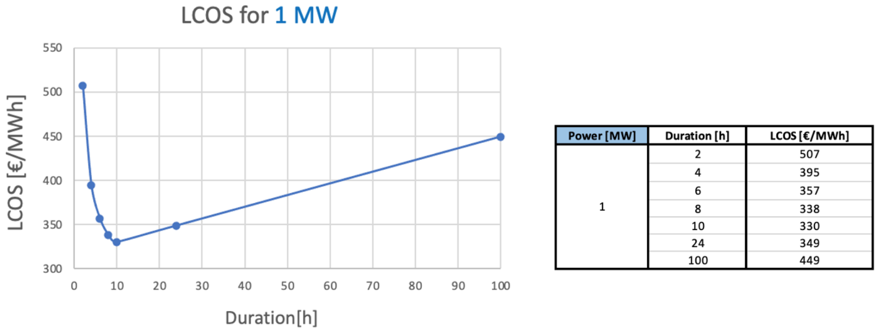

Power [MW]	Duration [h]	LCOS [€/MWh]
1	2	507
	4	395
	6	357
	8	338
	10	330
	24	349
	100	449

(a) LCOS results, 1 MW

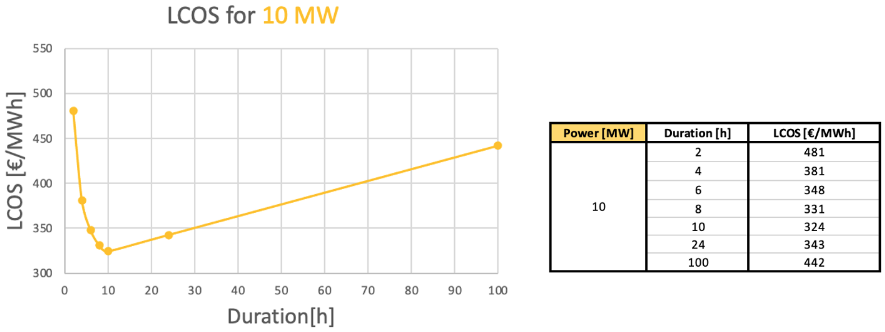

Power [MW]	Duration [h]	LCOS [€/MWh]
10	2	481
	4	381
	6	348
	8	331
	10	324
	24	343
	100	442

(b) LCOS results, 10 MW

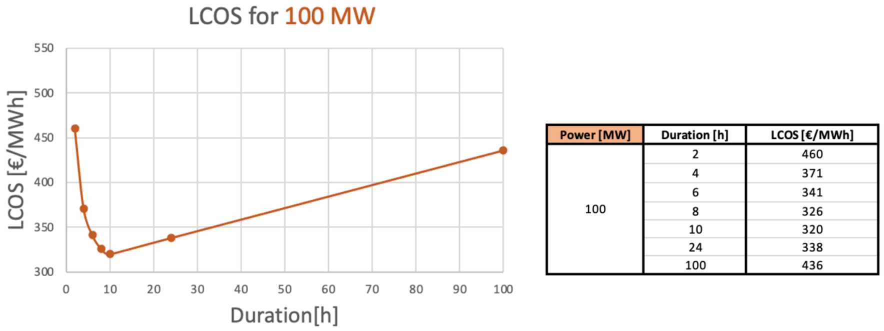

Power [MW]	Duration [h]	LCOS [€/MWh]
100	2	460
	4	371
	6	341
	8	326
	10	320
	24	338
	100	436

(c) LCOS results, 100 MW

Figure 3.21: LCOS results at different duration applications, for 1, 10 and 100 MW. The most competitive solutions include nominal discharge duration between 8 and 10 hours, where the energy factor is the dominant contribution over the expenditures factors. In these duration timeframes, the LCOS value is minimized. After 10 hours, the costs increase become predominant, causing a consequent aigmentation of the LCOS. Moreover, an increase of power size brings a further reduction of the costs, mostly due to economy of scale effects.

Even if the obtained results are currently not competitive with respect to more traditional Lithium-ion batteries (with an average LCOS between 200 and 250

€/MWh, for energy applications), this work's calculations showed the cost ranges where AORFB costs are more economically convenient. Moreover, the optimal discharge timeframe highlighted here, together with the longer lifetime of redox batteries with respect to Lithium technology, open interesting market possibilities for AORFBs in LDES applications in the upcoming future.

Chapter 4

Conclusions

This work has shown the operational performances of a prototypal AORFB device system. An experimental campaign has been undertaken, to investigate the battery device's behavior for both high DOD and reduced SOC ranges, showing the system's operating stability and energy efficiencies in both these conditions, for different C-rates and SOC ranges operations.
For high DOD tests, better performances have been recorded for prolonged operative timeframes, proving that AORFBs' true potential emerges for longer operations, thus confirming that redox-flow technology shows absolutely suitable conditions to support long-duration energy storage solutions.
The recorded DC efficiency values are above 82% for every examines C-rate condition, with the only exception of C/1, with an average efficiency value of 72%. This efficiency reduction is supposedly due to diffusion phenomena, enhanced by high current, with a possible increase of organic molecules' crossover mechanisms and consequent reduction of energy performance. During longer experimental tests, the observed auxiliary consumption during operation at different power rates has highlighted the necessity for an optimal system's design implementation, such as modular pumping devices. This is crucial to have more proportional auxiliary consumption with respect to the required power application, rather than a higher base load, constant throughout the battery's operation. Consequently, the auxiliary consumption's reduction will maximize the global system's efficiency.

The experimental tests performed at reduced SOC intervals have verified very similar DC performance results, for respective power rates,for the three examined SOC ranges of 20-30%, 50-60%, and 80-90%. Between these intervals, the average difference in efficiencies recorded values within 1%.
Similar considerations arise for AC values: not considering effects due to the system's derating, the recorded results are quite consistent, among different test at low SOC results as well as with respect to high DOD tests.

Both these tests' typologies have proven how the major influence on the AORFB device's operational behavior resides in the operational power rate, rather than in the operational SOC interval.

A techno-economic analysis has been evaluated, showing how AORFB are expected to be competitive with VRFB systems, once organic batteries reach the same roundtrip efficiency value as VRFB of 65%, which is expected to be obtained in less than five years since this work's completion.
This work's experimental campaign has proved the operative stability of the explored technology, while the techno-economic results have showed the current AORFBs' costs and efficiency parameters, to incentive the feasibility of these battery systems.
With devices designed for eight or ten hours, the minimum levelized cost of storage is obtained. For the optimal duration ranges between eight and ten hours, the minimum LCOS results evaluated in this work range between 340 and 320 €/MWh. Obviously, AORFBs are currently still more expensive than traditional battery technologies, especially compared to Lithium batteries (with usual LCOS values between 200 and 250 €/MWh).
However, the promising redox batteries' cycle life opens interesting market possibilities for stationary storage solutions, for energy plants with operational life incompatible with traditional electrochemical systems, but totally suitable for RFBs' characteristics.
Moreover, the optimal duration timeframe perfectly fits the long-duration energy storage conditions, and it represents actual evidence that AORFB devices constitute an absolutely valid long-term solution, to enhance the development of renewable energy sources on an industrial global scale.

Appendix A

Techno-economic features

This section indicates the specific values of the financial elements used in the techno-economic calculations.
A fundamental financial parameter is the weighted average cost of capital ($WACC_{\text{real}}$), which is necessary in the CAPEX equation 2.10. The expression of $WACC_{\text{real}}$ is indicated here:

$$WACC_{\text{real}} = \frac{1 + WACC_{\text{nominal}}}{1 + inflation} \tag{A.1}$$

$$WACC_{\text{nominal}} = DF \cdot i_{\text{nom}} \cdot (1 - \tau) + (1 - DF) \cdot COE_{\text{nom}} \tag{A.2}$$

The values needed for WACC's calculations are the following:

1. Nominal cost of equity [44].
2. Debt fraction [45].
3. Inflation rate [44].
4. Nomnial interest rate [45].
5. Tax rate [46].

The above listed parameters' values used in the techno-economic evaluation are are indicated in A.1.

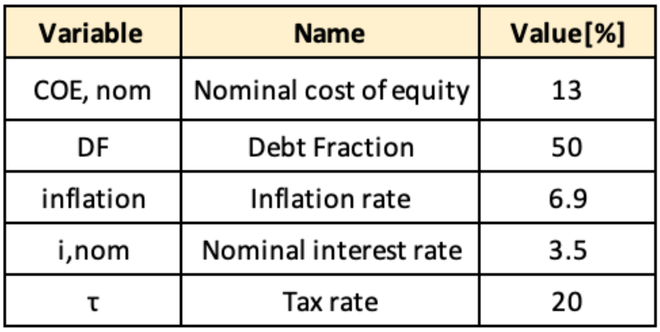

Variable	Name	Value[%]
COE, nom	Nominal cost of equity	13
DF	Debt Fraction	50
inflation	Inflation rate	6.9
i,nom	Nominal interest rate	3.5
τ	Tax rate	20

Figure A.1: WACC parameters values

The last used financial parameters is the rate of discount r_b for batteries used in 2.12 and 2.13 is equal to 8% [47].

Appendix B

Python Code

```python
    import os
    os.system("echo 1")
    # Techno-economic model

x = [1, 10, 100]  # Power size
t_nom = 4   # [h], reference duration for cost invoices of PNNL

# Cost invoices values, from PNNL reference
SB = [276.59, 263.42, 250.24]  # [$/kWh]
z_bos = [55.32, 52.68, 52.55]  # [$/kWh]
z_syin = [56.34, 52.55, 49.38]  # [$/kWh]

# Electrolyte costs
ELY_VRFB = 151.86  # [$/kWh]
ELY_AORFB_norm = 36.36  # [$/kWh]
ELY_delta = ELY_VRFB - ELY_AORFB_norm  # [$/kWh]

z_sb = [0, 0, 0]
for i in range(0, 3):
    z_sb[i] = SB[i] - ELY_delta  # SB del moxdello AORFB, [$/kWh]

N_proj = 20  # Project lifetime
n = int(100)
om_coeffs = [0.0043, 0.3]

pump_perc = 0.05
tank_perc = 0.02

# economic params
infl = 0.069  # EU, US: infl= 0.028
i_nom = 0.035  # EU, US: i_nom = 0.08
```

```python
DF = 0.5   # Debt fraction
tau = 0.2   # Tax coeffient
COE_nom, COE_real = 0.13, 0.0992  # Coefficients of equity
WACC_nom = DF*i_nom*(1-tau)+(1-DF)*COE_nom  # Weighted average cost of capital
WACC_real = ((1+WACC_nom)/(1+infl))-1
d = WACC_real
r_disc = 0.08  # rate of discount for energy storage projects
p_elec_eur = 0.175  # Electricity charging cost, [ /kWh]
financial_conversion = 0.926097425  # [ /$], April 2023

DOD = 0.8  # Depth of discharge
RTE = 0.65  # Roundtrip efficiency
Cycle_max_year = 365  # Assumed maximum cycles per year, as in HYBRIS reference
Degr_year = 0.01  # Yearly degradation in AORFB


# Trend function for SB, BOS, and System Integration
def func(x, a, b):
    return a*pow(x, b)
# np.exp() works with scalars, math.exp() only with scalar
sb_st_cf = [160.27, -0.0389]
bos_st_cf = [55.32, -0.0217]
syin_st_cf = [56.2792, -0.0287]
# Lower lims:
# upper lims=
# *popt = coeffs
# print(popt_sb)
# Extract the fitting parameters

# get individual data of z
NewX = float(input('Prated [MW]: '))
NewY = float(input('Duration [h]: '))  #keep Duration as Y, but Z does NOT depend on Y
#Energy depends on new Duration; Costs are all referred to y=4h

En_rat = NewX*NewY  # MWh
Z_sb = func(NewX, *sb_st_cf)  # $/kWh, *popt = coeffs
Z_bos = func(NewX, *bos_st_cf)  # $/kWh
Z_syin = func(NewX, *syin_st_cf)  # $/kWh
print(f'In AORFB, SB: {Z_sb} [$/kWh],BOS: {Z_bos} [$/kWh],System Integration: {Z_syin} [$/kWh] ')  # [$/kWh]
# Power conversion system (PCS) invoices conditions, as shown in PNNL reference
if NewX < 10:
     PCS = 85
elif 10 <= NewX < 100:
     PCS = 73
```

```
elif NewX >= 100:
    PCS = 61

# DC/DC converter (DCDC) invoice conditions , as shown in PNNL reference
if NewX < 10:
    DCDC = 69.86
elif 10 <= NewX < 100:
    DCDC = 60
elif NewX >= 100:
    DCDC = 53.78

# Control & Communication (CC) invoice conditions, as shown in PNNL reference
if NewX < 10:
    CC = 40
elif 10 <= NewX < 100:
    CC = 7.8
elif NewX >= 100:
    CC = 1.5

# Initial Cash flow (CF0): reference for pumps and tanks
CF_0_norm = (Z_sb + Z_bos + Z_syin) + (DCDC + PCS + CC)/t_nom  # $/kWh, normalized to 4h
Pumps = pump_perc*CF_0_norm  # $/kW

Tanks_norm = tank_perc*CF_0_norm  # $/kWh, tank size for 4 ore
Tanks = Tanks_norm*NewY      # $/kW, tanks size for new input discharge duration

Stack = Z_sb - Tanks_norm - ELY_AORFB_norm  # $/kWh, stack size for 4 h
ELY_AORFB = ELY_AORFB_norm*NewY  # $/kW, ELY cost for new discharge duration

Z_sb_DUR = Stack*t_nom + Tanks + ELY_AORFB   # $/kW, to have coherent unit of measures
CF_0 = Z_sb_DUR + (Z_bos + Z_syin)*t_nom + (DCDC + PCS + CC)  # $/kW
# PCS:
OM = om_coeffs[0]*CF_0 + om_coeffs[1]*PCS/N_proj   # Opex, [$/kW]
print(f'CF0: {round(CF_0 ,3)}[$/kW], Pumps costs: {round(Pumps,3)}[$/kW]')  # $/kW
print(f'Tanks costs: {round(Tanks,3)}[$/kW]')  # $/kW

Repl = Stack*t_nom + Pumps  # Replace costs, [$/kW]

CF_start = [CF_0, 0, 0, 0, 0, 0, 0, 0, 0, 0, 0, 0, Repl, 0, 0, 0, 0, 0, 0, 0]  # $/kW
CF = [0, 0, 0, 0, 0, 0, 0, 0, 0, 0, 0, 0, 0, 0, 0, 0, 0, 0, 0, 0]
```

```
Deflation = [0, 0, 0, 0, 0, 0, 0, 0, 0, 0, 0, 0, 0, 0, 0, 0, 0, 0, 0, 0, 0]
Def_degr = [0, 0, 0, 0, 0, 0, 0, 0, 0, 0, 0, 0, 0, 0, 0, 0, 0, 0, 0, 0, 0]
# print(CF_0, Repl)  # $/kW

# CF formula
for i in range(20):  # reduced from 24 to 20 years
    CF[i] = CF_start[i]/((1+d)**i)  # $/kW

for i in range(1, 21):  # reduced from 24 to 20 years
    Deflation[i] = 1/((1+r_disc)**i)  # Deflation coefficient
    Def_degr[i] = (1-Degr_year*i)*Deflation[i]  # Deflation-degradation coefficient


Capex, DEFLATION, DEF_DEGR = sum(CF), sum(Deflation), sum(Def_degr)  # Capex in $/kW
print(f'Degradation: {DEF_DEGR} ')
CAPEX = (Capex*NewX*1000)*financial_conversion  # [ ]
OPEX = OM*NewX*1000*financial_conversion  # [ , per year]

print(f'Capex: {float(CAPEX/1000000)}[million ], Opex: {int(OPEX)}[ per year]')  # $/kW, con errore capex < 3%

DT = DOD*NewY  # discharging time, dependent on new duration
CT = DT/RTE  # charging time
# Cycles calculation
cyc_eq_day = 1/DOD
cyc_day_poss = (24/(CT+DT))
cyc_max = min((1/DOD), cyc_day_poss)
cyc_annual = cyc_max*Cycle_max_year
print(f'cycles annual: {cyc_annual}, Disch time: {DT} [h], Charging time: {CT}[h]')
E_batt = cyc_annual*En_rat*1000*DOD*DEF_DEGR  # Energy discharged by the battery,[kWh]
LCOS = (CAPEX + OPEX*DEFLATION+(p_elec_eur*E_batt/RTE))/E_batt  # Levelized cost of storage [ /kWh]
print(f'Energy produced yearly by battery: {int(E_batt)}[KWh]')
print(f'Levelized cost of storage: {round(LCOS,6)} [ /kWh]')
```

Bibliography

[1] IEA - International Energy Agency. *World Energy Outlook 2022*. 2022. URL: `https://www.iea.org/reports/world-energy-outlook-%2022` (cit. on pp. 2, 8).

[2] Dolf Gielen, Francisco Boshell, Deger Saygin, Morgan D Bazilian, Nicholas Wagner, and Ricardo Gorini. «The role of renewable energy in the global energy transformation». In: *Energy strategy reviews* 24 (2019), pp. 38–50 (cit. on p. 2).

[3] Dolf Gielen, Francisco Boshell, Deger Saygin, Morgan D Bazilian, Nicholas Wagner, and Ricardo Gorini. «Energy Strategy Reviews». In: (2019) (cit. on p. 2).

[4] IEA - International Energy Agency. *Renewables 2022*. 2022. URL: `https://l1nq.com/W2Hzw` (cit. on pp. 2, 3).

[5] Arnulf Jäger-Waldau et al. «PV status report 2019». In: *Publications Office of the European Union: Luxembourg* (2019), pp. 7–94 (cit. on p. 2).

[6] Manish Ram, Michael Child, Arman Aghahosseini, Dmitrii Bogdanov, Alena Lohrmann, and Christian Breyer. «A comparative analysis of electricity generation costs from renewable, fossil fuel and nuclear sources in G20 countries for the period 2015-2030». In: *Journal of cleaner production* 199 (2018), pp. 687–704 (cit. on p. 2).

[7] Aleh Cherp, Vadim Vinichenko, Jale Tosun, Joel A Gordon, and Jessica Jewell. «National growth dynamics of wind and solar power compared to the growth required for global climate targets». In: *Nature Energy* 6.7 (2021), pp. 742–754 (cit. on p. 2).

[8] Carolina Koronen, Max Åhman, and Lars J Nilsson. «Data centres in future European energy systems—energy efficiency, integration and policy». In: *Energy Efficiency* 13.1 (2020), pp. 129–144 (cit. on p. 3).

[9] Katie Jost and George Xydis. «Offshore wind acceleration in the US Atlantic coast and the 30 GW by 2030 target». In: *Proceedings of the Institution of Civil Engineers-Energy* (2023), pp. 1–8 (cit. on p. 3).

[10] *European Association for Storage of Energy - Energy Storage Targets 2030 and 2050, ensuring Europe's energy security in a Renewable Energy System.* `https://shorturl.at/fnrxX`. 2022 (cit. on p. 5).

[11] C Opathella, Ayman Elkasrawy, Amr A Mohamed, and B Venkatesh. «Optimal scheduling of merchant-owned energy storage systems with multiple ancillary services». In: *IEEE Open Access Journal of Power and Energy* 7 (2019), pp. 31–40 (cit. on p. 5).

[12] Patrick T Moseley and Jurgen Garche. *Electrochemical energy storage for renewable sources and grid balancing.* Newnes, 2014 (cit. on p. 5).

[13] Emiliano Borri, Gabriel Zsembinszki, and Luisa F Cabeza. «Recent developments of thermal energy storage applications in the built environment: A bibliometric analysis and systematic review». In: *Applied Thermal Engineering* 189 (2021), p. 116666 (cit. on p. 5).

[14] Md Mustafizur Rahman, Abayomi Olufemi Oni, Eskinder Gemechu, and Amit Kumar. «Assessment of energy storage technologies: A review». In: *Energy Conversion and Management* 223 (2020), p. 113295 (cit. on p. 5).

[15] Tyler S Mathis, Narendra Kurra, Xuehang Wang, David Pinto, Patrice Simon, and Yury Gogotsi. «Energy storage data reporting in perspective—guidelines for interpreting the performance of electrochemical energy storage systems». In: *Advanced Energy Materials* 9.39 (2019), p. 1902007 (cit. on p. 6).

[16] Suresh Sagadevan, AR Marlinda, Zaira Zaman Chowdhury, Yasmin Binti Abdul Wahab, Nor Aliya Hamizi, MM Shahid, Faruq Mohammad, Jiban Podder, and Mohd Rafie Johan. «Fundamental electrochemical energy storage systems». In: *Advances in Supercapacitor and Supercapattery.* Elsevier, 2021, pp. 27–43 (cit. on p. 6).

[17] Thilo Bocklisch. «Hybrid energy storage approach for renewable energy applications». In: *Journal of Energy Storage* 8 (2016), pp. 311–319 (cit. on p. 7).

[18] Thandavarayan Maiyalagan and Perumal Elumalai. *Rechargeable lithium-ion batteries: trends and progress in electric vehicles.* CRC Press, 2020 (cit. on p. 7).

[19] Eduard Bullich-Massagué, Francisco-Javier Cifuentes-Garcıa, Ignacio Glenny-Crende, Marc Cheah-Mañé, Mònica Aragüés-Peñalba, Francisco Dıaz-González, and Oriol Gomis-Bellmunt. «A review of energy storage technologies for large scale photovoltaic power plants». In: *Applied Energy* 274 (2020), p. 115213 (cit. on p. 7).

[20] Jose I Leon, Eugenio Dominguez, Ligang Wu, Abraham Marquez Alcaide, Manuel Reyes, and Jianxing Liu. «Hybrid energy storage systems: Concepts, advantages, and applications». In: *IEEE Industrial Electronics Magazine* 15.1 (2020), pp. 74–88 (cit. on p. 7).

[21] MA Hannan, SB Wali, PJ Ker, MS Abd Rahman, M Mansor, VK Ramachandaramurthy, KM Muttaqi, TMI Mahlia, and ZY Dong. «Battery energy-storage system: A review of technologies, optimization objectives, constraints, approaches, and outstanding issues». In: *Journal of Energy Storage* 42 (2021), p. 103023 (cit. on p. 8).

[22] Alberto Grimaldi, Francesco Demetrio Minuto, Alessandro Perol, Silvia Casagrande, and Andrea Lanzini. «Ageing and energy performance analysis of a utility-scale lithium-ion battery for power grid applications through a data-driven empirical modelling approach». In: *Journal of Energy Storage* 65 (2023), p. 107232 (cit. on p. 8).

[23] A Bettoli, M Linder, T Nauclér, J Noffsinger, S Sengupta, H Tai, and G van Gendt. «Net-zero power: Long-duration energy storage for a renewable grid». In: *McKinsey & Company, November* 22 (2021) (cit. on p. 8).

[24] Paul Albertus, Joseph S Manser, and Scott Litzelman. «Long-duration electricity storage applications, economics, and technologies». In: *Joule* 4.1 (2020), pp. 21–32 (cit. on p. 8).

[25] Bjarne Steffen, Tyeler Matsuo, Davita Steinemann, and Tobias S Schmidt. «Opening new markets for clean energy: The role of project developers in the global diffusion of renewable energy technologies». In: *Business and Politics* 20.4 (2018), pp. 553–587 (cit. on p. 8).

[26] M Rychcik and M Skyllas-Kazacos. «Characteristics of a new all-vanadium redox flow battery». In: *Journal of power sources* 22.1 (1988), pp. 59–67 (cit. on p. 8).

[27] Jan Girschik, Lukas Kopietz, Michael Joemann, Anna Grevé, and Christian Doetsch. «Redox flow batteries: stationary energy storages with potential». In: *Chemie Ingenieur Technik* 93.4 (2021), pp. 523–533 (cit. on p. 8).

[28] Loıs Briot, Martin Petit, Quentin Cacciuttolo, and Marie-Cécile Pera. «Aging phenomena and their modelling in aqueous organic redox flow batteries: A review». In: *Journal of Power Sources* 536 (2022), p. 231427 (cit. on pp. 8, 10, 17, 18, 20).

[29] Mengqi Gao, Zhiyu Wang, Dao Gen Lek, and Qing Wang. «Towards high power density aqueous redox flow batteries». In: *Nano Research Energy* 2.1 (2023), e9120045 (cit. on pp. 9, 14–16, 18, 52).

[30] Rui Shan, Jeremiah Reagan, Sergio Castellanos, Sarah Kurtz, and Noah Kittner. «Evaluating emerging long-duration energy storage technologies». In: *Renewable and Sustainable Energy Reviews* 159 (2022), p. 112240 (cit. on p. 12).

[31] Anuoluwapo Aluko and Andy Knight. «A Review on Vanadium Redox Flow Battery Storage Systems for Large-Scale Power Systems Application». In: *IEEE Access* (2023) (cit. on p. 12).

[32] Vilayanur Viswanathan, Kendall Mongird, Ryan Franks, and Richard Baxter. «2022 Grid Energy Storage Technology Cost and Performance Assessment». In: *Energy* 2022 (2022) (cit. on pp. 15, 33–35, 39–41, 43, 51, 60).

[33] Faizur Rahman and M Skyllas-Kazacos. «Evaluation of additive formulations to inhibit precipitation of positive electrolyte in vanadium battery». In: *Journal of Power Sources* 340 (2017), pp. 139–149 (cit. on p. 17).

[34] Nawin Ra and Ankur Bhattacharjee. «An extensive study and analysis of system modeling and interfacing of vanadium redox flow battery». In: *Energy Technology* 9.1 (2021), p. 2000708 (cit. on p. 17).

[35] L Tang, P Leung, MR Mohamed, Q Xu, S Dai, X Zhu, C Flox, AA Shah, and Q Liao. «Capital cost evaluation of conventional and emerging redox flow batteries for grid storage applications». In: *Electrochimica Acta* 437 (2023), p. 141460 (cit. on p. 19).

[36] Pacific Northwest National L. *Vanadium Redox flow batteries*. `https://www.pnnl.gov/vanadium-redox-flow-battery`. 2022 (cit. on p. 33).

[37] Vilayanur Viswanathan et al. «Cost and performance model for redox flow batteries». In: *Journal of Power Sources* 247 (2014), pp. 1040–1051 (cit. on pp. 34, 35, 37, 39).

[38] *HYBRIS project deliverables and publications*. `https://www.pnnl.gov/lcos-estimates`. 2022 (cit. on pp. 41, 61).

[39] Gestore Mercati Energetici. *dati di sintesi MPE-MGP*. 2022. URL: `https://www.mercatoelettrico.org/It/Statistiche/ME/DatiSintesi.aspx` (cit. on p. 41).

[40] Igor Derr, Abdulmonem Fetyan, Konstantin Schutjajew, and Christina Roth. «Electrochemical analysis of the performance loss in all vanadium redox flow batteries using different cut-off voltages». In: *Electrochimica Acta* 224 (2017), pp. 9–16 (cit. on p. 45).

[41] Tao Zou, Xiaohu Shi, and Longhai Yu. «Study on energy loss of 35 kW all vanadium redox flow battery energy storage system under closed-loop flow strategy». In: *Journal of Power Sources* 490 (2021), p. 229514 (cit. on p. 51).

[42] Politecnico di Milano Giuliano Rancilio Dipartimento di Energia. *Modellazione, pianificazione ed esercizio di sistemi di accumulo a batteria.* 2023. URL: `http://www.e4g.polimi.it/wp-content/uploads/2303_ModellazioneBESS_gruppoSistemiElettriciEnergia_POLIMI.pdf` (cit. on pp. 56, 58).

[43] Pacific Northwest National L. *Energy Storage LCOS estimates.* `https://www.pnnl.gov/lcos-estimates`. 2022 (cit. on p. 63).

[44] Eurostat. *Euroindicators.* 2023. URL: `https://ec.europa.eu/eurostat/documents/2995521/16324747/2-31032023-AP-EN.pdf/e1ba8561-cfa9-6734-3be3-e0ca47d635b6` (cit. on p. 70).

[45] Data browser Eurostat. *HICP at constant tax rates - monthly rate of change.* 2023. URL: `https://ec.europa.eu/eurostat/databrowser/view/prc_hicp_cmon/default/table?lang=en` (cit. on p. 70).

[46] Data browser Eurostat. *Tax revenue statistics.* 2023. URL: `https://ec.europa.eu/eurostat/statistics-explained/index.php?title=Tax_revenue_statistics` (cit. on p. 70).

[47] IEA. *Projected Costs of Generating Electricity.* 2020. URL: `https://www.iea.org/reports/projected-costs-of-generating-electricity-2020` (cit. on p. 71).